

1 Nitrogen cycling in the Southern Ocean Kerguelen Plateau area:
2 Evidence for significant surface nitrification from nitrate isotopic
3 compositions

4

5 F. Dehairs¹, F. Fripiat¹, A.-J. Cavagna¹, T.W. Trull^{2,3,4}, C. Fernandez^{5,6}, D. Davies,^{2,3},
6 A. Roukaerts¹, D. Fonseca Batista¹, F. Planchon⁷ and M. Elskens¹

7

- 8 1. Analytical, Environmental and Geo – Chemistry; Earth Sciences Research Group,
9 Vrije Universiteit Brussel, Belgium
10 2. CSIRO Marine and Atmospheric Research, Hobart, Tasmania, Australia
11 3. Antarctic Climate and Ecosystems Cooperative Research Centre, Hobart,
12 Tasmania, Australia
13 4. Institute for Marine and Antarctic Studies, University of Tasmania, Hobart,
14 Tasmania, Australia
15 5. Sorbonne Universités, UPMC Univ Paris 06, UMR7621, Laboratoire
16 d’Océanographie Microbienne, Observatoire Océanologique, F-66650
17 Banyuls/mer, France
18 6. Department of Oceanography, COPAS SurAustral program and Interdisciplinary
19 center for Aquaculture Research (INCAR), University of Concepción, Chile.
20 7. Laboratoire des Sciences de l’Environnement Marin (LEMAR) Université de
21 Bretagne Occidentale, Institut Européen de la Mer, Plouzané, Brest, France

22

23 Corresponding author: fdehairs@vub.ac.be

24

25

26 Running title: Nitrogen cycling in the Southern Ocean

27 Abstract

28 This paper presents whole water column data for nitrate N, O isotopic composition for
29 the Kerguelen Plateau area and the basin extending east of the Island, aiming at
30 understanding the N-cycling in this naturally iron fertilized area that is characterized by
31 large re-current phytoplankton blooms. The KEOPS 2 expedition (Oct.-Nov. 2011) took
32 place in spring season and complements knowledge gathered during an earlier
33 summer expedition to the same area (KEOPS 1, Feb.-Mar. 2005). As noted by others a
34 remarkable condition of the system is the moderate consumption of nitrate over the
35 season (nitrate remains > 20 μM) while silicic acid becomes depleted, suggesting
36 significant recycling of nitrogen. Nitrate isotopic signatures in the upper water column
37 do mimic this condition, with surprising overlap of spring and summer regressions of
38 $\delta^{18}\text{O}_{\text{NO}_3}$ vs. $\delta^{15}\text{N}_{\text{NO}_3}$ isotopic compositions. These regressions obey rather closely the
39 $^{18}\epsilon/^{15}\epsilon$ discrimination expected for nitrate uptake ($^{18}\epsilon/^{15}\epsilon = 1$), but regression slopes as
40 large as 1.6 were observed for the mixed layer above the Kerguelen Plateau. A
41 preliminarily mass balance calculation for the early bloom period points toward
42 significant nitrification occurring in the mixed layer and which be equivalent to some
43 80% of nitrate uptake above the Kerguelen Plateau. A further finding concerns deep
44 ocean low $\delta^{18}\text{O}_{\text{NO}_3}$ values (<2‰) underlying high chlorophyll waters at the Polar Front
45 Zone and which cannot be explained by remineralisation and nitrification of the local
46 particulate nitrogen flux, which is too small in magnitude. However, the studied area is
47 characterised by a complex recirculation pattern that would keep deep waters in the
48 area and could impose a seasonally integrated signature of surface water processes on
49 the deep waters.

50

51

52 1. Introduction

53 The Kerguelen Plateau and lee-ward off-shelf areas are characterized by intense
54 seasonal phytoplankton blooms, which are sustained by enhanced iron supply from
55 deep water (Blain et al., 2007; 2008). While these intense blooms result in strong silicic
56 acid depletion, their impact on depletion of the nitrate stocks is much smaller, with
57 end-of-bloom surface water nitrate concentrations still very high, as observed during
58 the KEOPS 1 expedition in late summer 2005 (Blain et al. 2007; Mosseri et al., 2008).
59 Relative to the magnitude of primary production the bloom areas are characterized by
60 enhanced shallow remineralisation and reduced deep sea export, as compared to off-
61 shelf areas located outside the bloom patch (Jacquet et al., 2008). Mosseri et al. (2008)
62 report that despite similar silicic acid and nitrate uptake ratios being close to 1, the
63 apparent nitrate consumption over the season was much lower than the silicic acid
64 consumption, implying significant shallow remineralisation of N, as evidenced by
65 substantial sub-surface ammonium concentrations, reaching up to 2 μM (Mosseri et
66 al., 2008). It is likely that such conditions would also favor a surface ocean
67 development of nitrifying Bacteria and Archaea, with some members of the latter
68 group known to have affinities for ammonium equaling and even exceeding those of
69 diatoms (Martens-Habbena et al., 2009; Stahl and de la Torre, 2012).

70 Several authors have highlighted that knowledge about nitrate stable isotope
71 composition is an essential asset to resolve the complex suite of processes that control
72 the oceanic N cycle (see e.g., Sigman et al., 1999; DiFiore et al., 2006; 2009; Rafter et
73 al., 2013). During the early season KEOPS 2 expedition (Oct.-Nov.) to the Kerguelen
74 area, we analysed the N and O stable isotope composition of nitrate over the whole
75 water column to investigate possible imprints of the above described shallow
76 remineralisation + nitrification process, as well as imprints of enhanced primary
77 production on deep ocean nitrate isotopic composition. Furthermore, this early season
78 expedition offered the opportunity to investigate the seasonal variability of the nitrate
79 isotopic composition, by comparing results with those obtained earlier by others
80 during the late summer KEOPS 1 expedition to the same area (Trull et al., 2008). This

81 work on nitrate isotopic composition takes advantage of the study of primary
82 production, nitrate and ammonium uptake, carbon export production and
83 remineralization that was conducted by others during the KEOPS 2 expedition
84 (Cavagna et al., 2014; Planchon et al., 2014 and Jacquet et al., 2014).

85 Confirming previous studies, combined measurement of nitrate dual isotope
86 composition and N-nutrient uptake rate measurements, as performed during KEOPS 2,
87 appears to be particularly useful for investigating surface ocean N-processes. In that
88 aspect this study differs from previous studies on nitrogen cycling using the natural
89 nitrate dual isotopic composition, but lacking information on N-process rates. The
90 present study also adds significantly to the existing data base on nitrate isotopic
91 composition in the Southern Ocean, with new data for the Polar Front region in a
92 naturally iron fertilized area.

93

94 2. Methods

95 2.1 Site description

96 The studied area covers the broad plateau region stretching between Kerguelen and
97 Heard Island to the SE, and the deep basin to the east of the island (Figure 1). This
98 basin is bound to the south by the Kerguelen Plateau and to the north by a sill (Gallieni
99 Spur) extending from the plateau in north-easterly direction (Figure 1).

100 Briefly, the studied area to the east of Kerguelen is crossed by the meandering Polar
101 Front, which circumvents the island from the south-west, crosses the shallow (~500m)
102 Kerguelen Plateau (which extends in south easterly direction from the island) and
103 forms a loop extending northward till the sill that borders the basin to the north
104 (Gallieni Spur), thereby enclosing a stable mesoscale meander structure (Figure 1).
105 Surface and subsurface waters closely follow, and actually define the position of the
106 PF. Deep water flow in the area is fed by Circumpolar Deep water flow channeled
107 through the Fawn Trough (Park et al., 2008) and also by the northward directed deep

108 western boundary current in the Australian Antarctic basin east of the Kerguelen
109 Plateau (McCartney and Donohue, 2007; Fukamachi et al., 2010).

110 For further details about the topography and the large scale circulation in the
111 Kerguelen Island and Plateau areas we refer to Park et al. (2008).

112 The T-S diagram (Figure 1) highlights the hydrodynamic environment of the Kerguelen
113 area, with profiles characteristic of the Open Ocean Zone. Most salient features are:
114 highest temperatures in surface waters; presence of subsurface temperature minimum
115 Winter Water; increased temperatures in Upper Circumpolar Deep Water; increased
116 salinities in Lower Circumpolar Deep Water; a broad salinity maximum reflecting the
117 remnant North Atlantic Deep Water; slightly less saline and cold Bottom Waters.

118 *2.2 Sampling and Analysis*

119 The KEOPS 2 expedition took place from Oct. till early Nov. 2011 on board R/V Marion
120 Dufresne. The sampling strategy aimed at documenting both the short term temporal
121 evolution of the system during pre- and bloom conditions of selected sites and the
122 broader spatial variability between Plateau and more off-shelf sites (Figure 1b shows
123 the map with the MODIS Chlorophyll pattern superimposed). Short term temporal
124 evolution was followed in a stationary meander of the Polar Front and by revisiting
125 sites above the Plateau, while spatial variability was studied along a W - E section and a
126 N - S section covering the Plateau and the basin east of Kerguelen Island.

127 The water column was sampled per CTD rosette equipped with 12L Niskin bottles. N-
128 nutrients (nitrate, nitrite, ammonium) were measured onboard using classical
129 spectrophotometric methods (Blain et al. 2014). The samples for nitrate isotopic
130 composition consisted of a sub-fraction (10 ml) of the filtered seawater (Acrodisc; 0.2
131 μm porosity) intended for on-board nitrate + nitrite analysis. These subsamples were
132 kept frozen (-20°C) till analysis in the home-based laboratory. The nitrogen and oxygen
133 isotopic composition of nitrate was determined via the bacterial denitrifier method,
134 using *Pseudomonas aureofaciens* bacteria which reduce nitrate to N_2O (Sigman et al.,
135 2001; Casciotti et al., 2002). We aimed at a final homogenous nitrate content of 20

136 nmoles for samples and reference standards alike (see below). The analytical
137 equipment consisted of a custom-build gas bench connected on-line to a set-up for gas
138 conditioning, which involved elimination of volatile organic carbon compounds, CO₂
139 and cryogenic focusing of N₂O, GC separation of CO₂ traces from N₂O, a Con-Flo unit
140 and IRMS (Thermo Delta V). For final calculations we used the USGS 32, 34, 35 and
141 IAEA N3 international reference standards (Sigman et al., 2001; Böhlke et al., 2003)
142 and the two-point normalization procedure as discussed in Casciotti et al. (2002) and
143 Paul et al. (2007). $\delta^{15}\text{N}$ values are reported as $[(^{15}\text{N}/^{14}\text{N})_{\text{sample}}/(^{14}\text{N}/^{15}\text{N})_{\text{ref}} - 1] * 1000$,
144 referenced to Air N₂ and $\delta^{18}\text{O}$ as $[(^{18}\text{O}/^{16}\text{O})_{\text{sample}}/(^{18}\text{O}/^{16}\text{O})_{\text{ref}} - 1] * 1000$, referenced to
145 VSMOW. Multiple analyses of USGS and IAEA reference solutions indicate average
146 measurement errors for $\delta^{15}\text{N}_{\text{NO}_3}$ and $\delta^{18}\text{O}_{\text{NO}_3}$ analyses were 0.17‰ and 0.38‰,
147 respectively. We also analysed 35 duplicate samples from successive CTD casts at same
148 depths yielding median values of the standard deviations being 0.05‰ and 0.28‰ for
149 $\delta^{15}\text{N}$ and $\delta^{18}\text{O}$, respectively.

150 Note that the method measures the isotopic composition of NO₃⁻ plus NO₂⁻. The
151 presence even of small nitrite amounts would lower the $\delta^{15}\text{N}$ and $\delta^{18}\text{O}$ values of
152 nitrate + nitrite relative to nitrate only (Casciotti et al., 2007). In the present study the
153 effect of NO₂⁻ was neglected since overall nitrite concentrations were small,
154 representing on average <0.5% of the nitrate + nitrite pool (see also DiFiore et al.,
155 2009). However, it has been reported that slightly higher nitrite levels reaching 0.8 %
156 of the nitrite + nitrate pool such as observed here for the surface waters can result in a
157 lowering of the $\delta^{15}\text{N}$ and $\delta^{18}\text{O}$ values by 0.4‰ and 0.2‰ on average (Rafter et al.,
158 2013; their supplementary material). We have not corrected our surface water nitrate
159 isotopic values for a possible nitrite effect, as is the case also in work presented by
160 others (see e.g., DiFiore et al. 2009; Rafter et al., 2013), but have considered the
161 impact of this when calculating nitrification (see section 4.5). Information on nitrate,
162 ammonium uptake experiments and C, N Export flux via the ²³⁴Th method is given in
163 the contributions by Cavagna et al. (2014) and Planchon et al. (2014). As part of the
164 analysis protocol for assessing carbon export via the ²³⁴Th method, we also analysed

165 $\delta^{15}\text{N}$ of suspended particulate nitrogen in the size fractions 1 to 53 μm and $> 53 \mu\text{m}$, as
166 sampled with large volume in-situ pumps (Planchon et al., 2014).

167

168 3. Results

169 The full data set ($\delta^{15}\text{N}_{\text{NO}_3}$, $\delta^{18}\text{O}_{\text{NO}_3}$, concentrations of NO_3^- , NO_2^- , NH_4^+ , Salinity, Tpot) is
170 available in Appendix Table 1.

171

172 3.1 Water column profiles

173 A total of 20 sites were sampled for analysis of nitrate isotopic composition. One site
174 located south-west of Kerguelen, in HNLC waters well outside the Kerguelen bloom
175 was taken as reference site (R-2; Table 1). We differentiate 3 regions (Table 1): (i)
176 Plateau stations located south of the PF, above the shallow Plateau and the margin
177 and underlying the bloom plume (stations A3-1, TNS8, TEW4, E4W1, A3-2, E4W2); (ii)
178 Polar Front Meander stations in the central part of the basin east of Kerguelen where
179 the bloom had not fully developed yet (stations TNS6, E1, TEW5, TEW6, E3, E4E, E5,
180 IODA-REC); (iii) Polar Front and north of Polar Front sites (stations TEW7, TEW8, F-L).
181 Average upper 100m Chl-a concentrations are highest for the Polar Front stations (2.03
182 $\pm 0.43 \mu\text{g l}^{-1}$), followed by the Plateau stations ($1.27 \pm 0.54 \mu\text{g l}^{-1}$), while the Meander
183 sites had lower Chl-a concentrations ($0.85 \pm 0.32 \mu\text{g l}^{-1}$), though clearly in excess of
184 values recorded for the HNLC reference station ($0.3 \mu\text{g l}^{-1}$) (Table 1). We note that
185 Plateau sites on average have the coldest ($2.27 \pm 0.34 \text{ }^\circ\text{C}$) and most saline (33.89
186 ± 0.02) surface waters (upper 100m), while PF sites have the warmest ($3.49 \pm 0.24 \text{ }^\circ\text{C}$)
187 and freshest (33.79 ± 0.02) surface waters (Table 1). Average nitrate values in the
188 upper 100m of water column remain high throughout the study period with average
189 values of 26.6 ± 1.9 ; 26.2 ± 0.9 and $23.1 \pm 1.3 \mu\text{M}$ for Plateau, Meander and PF areas,
190 respectively (Table 1). With increasing depth, nitrate concentrations in general
191 increase to reach maximal values around $37 \mu\text{M}$ at 500m in Upper Circumpolar Deep

192 waters (UCDW) (Figure 2a). Concentrations decrease slightly in Lower Circumpolar
193 Deep Waters (around 30 μM) and increase again slightly in bottom waters (around 32
194 μM). Profiles of $\delta^{15}\text{N}_{\text{NO}_3}$ mirror the ones of nitrate (Figure 2b): High values in surface
195 waters (reaching up to 7.5 ‰) which decrease to 4.6‰ in the NO_3^- maximum and
196 increase slightly to 5‰ till about 2500 m. A slight decrease of $\delta^{15}\text{N}_{\text{NO}_3}$ is noticed in
197 Polar Front bottom waters which also show a slight increase in nitrate concentration
198 (Figure 2a,b). Such values are similar to those observed widely for the deep ocean (see
199 Di-Fiore et al., 2009; Sigman et al., 2000; 2009b; Rafter et al., 2013). Although $\delta^{18}\text{O}_{\text{NO}_3}$
200 values are more scattered, it can be clearly seen that they follow a pattern similar to
201 $\delta^{15}\text{N}_{\text{NO}_3}$, with values up to 6‰ in surface waters, which decrease to <2‰ in the 500 to
202 1000m depth interval but tend to increase again in deep and bottom waters and stay
203 close to 2‰ (Figure 2c).

204 Differences of the $\delta^{15}\text{N}$ and $\delta^{18}\text{O}$ gradients between deep ocean and surface are
205 generally visualized by plotting the $\Delta(15-18)$ values, which have been defined (Sigman
206 et al., 2005) as: the difference between $\delta^{15}\text{N}$ and $\delta^{18}\text{O}$ (Rafter et al., 2013), keeping in
207 mind that for deep waters the $\delta^{15}\text{N}_{\text{NO}_3} - \delta^{18}\text{O}_{\text{NO}_3}$ difference is close to 3‰. From
208 Figure 2d it appears that surface waters have $\Delta(15-18)$ values generally <3‰ (range 0.9
209 - 3‰; average = $2.30 \pm 0.5\text{‰}$), with lowest values observed for Plateau, PF areas, and
210 Meander stations This indicates that surface water $\delta^{18}\text{O}$ values have increased more
211 than $\delta^{15}\text{N}$ values. In contrast, the sub-surface waters between 250 m and 1250 m show
212 a majority of data points with $\Delta(15-18)$ values > 3‰, though values are scattered rather
213 widely. Since uptake of nitrate fractionates $^{15}\text{N}/^{14}\text{N}$ and $^{18}\text{O}/^{16}\text{O}$ equally (Granger et al.,
214 2004; Sigman et al., 2005), another process needs to be invoked to explain the low
215 $\Delta(15-18)$ values for surface waters. In the discussion further below we show that these
216 low surface waters $\Delta(15-18)$ values (<3‰) can be attributed largely to a partial
217 utilization of the surface water nitrate pool combined with nitrification in the surface
218 and subsurface waters.

219 For the 250 m to 1500 m depth interval at stations on the PFZ side of the PF (east of
220 74°E) and to a lesser stations close to the plateau margin between 71° and 72°E (Figure

221 3a) we observe low $\delta^{18}\text{O}_{\text{NO}_3}$ values (<2‰) and high $\Delta(15-18)$ values(> 3‰; Figure 2d).
222 This feature is probably associated with advection of UCDW as discussed later. The
223 occurrence of these signals at the western and eastern borders of the meander
224 possibly reflects the presence of a cyclonic circulation in the basin which confines the
225 meander, as reported by Park et al. (2014). Note that the S to N section between
226 approximately 71° and 72°E also intersects the low $\delta^{18}\text{O}_{\text{NO}_3}$ waters (see Figure 3b).

227 Below 1500m $\Delta(15-18)$ values are close to 3‰, reflecting similar vertical gradients for
228 $\delta^{15}\text{N}$ and $\delta^{18}\text{O}$.

229

230 *3.2 W-E and S-N Sections*

231 Figure 3a,b shows the spatial distribution of the $\delta^{15}\text{N}_{\text{NO}_3}$ and $\delta^{18}\text{O}_{\text{NO}_3}$ signals and nitrate
232 concentration along the W to E and S to N transects. Deep waters (>500m) in the
233 central part of the W to E section, between 72°E and 74°E have $\delta^{15}\text{N}_{\text{NO}_3}$ values close to
234 5‰, while westward and eastward of this central area, deep waters have slightly lower
235 $\delta^{15}\text{N}$ values (Figure 3, top). Lowest $\delta^{15}\text{N}_{\text{NO}_3}$ values are observed in bottom waters
236 (>2000 m) east of 73°E and appear associated with very low temperatures (<1°C).
237 These waters are probably of southerly origin, associated with the Fawn Trough
238 Current, transporting cold Antarctic waters of eastern Enderby origin (Park et al., 2008)
239 and possibly also partly with the Deep Western Boundary Current which is part of the
240 deep cyclonic gyre in the Australian – Antarctic Basin (McCartney and Donohue, 2007;
241 Fukamachi et al., 2010).

242

243 4. Discussion

244 *4.1 Nitrate concentration and isotopic composition*

245 The clear ^{15}N , ^{18}O enrichments of nitrate in the upper ocean (Figure 2) suggest a strong
246 effect of isotopic discrimination during nitrate uptake by the phytoplankton (Sigman et

247 al., 1999; DiFiore et al., 2010). The isotope fractionation effect is visualized by plotting
248 $\delta^{15}\text{N}_{\text{NO}_3}$ and $\delta^{18}\text{O}_{\text{NO}_3}$ values vs. the natural logarithm of nitrate concentration (Figure
249 4). The degree of linearity of these relationships is indicative of the degree by which
250 isotopic discrimination approaches closed system Rayleigh fractionation. The slope
251 values of these regressions are equivalent to apparent discrimination factors
252 (ϵ). Whole water column values are -4.08 ± 0.17 (\pm se), -4.18 ± 0.20 and -4.54 ± 0.21 , for
253 Meander, Polar Front and Plateau areas, respectively (Figure 4). When focusing on the
254 upper 250m (this layer partly includes UCDW), slopes are slightly steeper, reaching -
255 4.62 ± 0.21 , -4.44 ± 0.23 and -4.76 ± 0.36 , respectively (Figure 4). Slopes for $\delta^{18}\text{O}_{\text{NO}_3}$ are
256 steeper than for $\delta^{15}\text{N}$, reaching -6.15 ± 0.37 , -6.20 ± 0.39 and -6.75 ± 0.56 for the whole
257 water column and -6.15 ± 0.87 , -5.18 ± 0.52 and -6.13 ± 1.03 , for the upper 250m, for
258 Meander, Polar Front and Plateau, respectively (Figure 4). We thus observe a tendency
259 for slopes of $\delta^{15}\text{N}_{\text{NO}_3}$ vs $\text{LN}[\text{NO}_3^-]$ to increase in shallow waters, while on the contrary
260 slopes for $\delta^{18}\text{O}_{\text{NO}_3}$ vs $\text{LN}[\text{NO}_3^-]$ decrease. Largest $\delta^{15}\text{N}$, $\delta^{18}\text{O}$ slope values are observed
261 for the Plateau sites. Overall such values fit within the range of ϵ values reported for
262 nitrate uptake by phytoplankton (4 - 10‰ for $^{15}\epsilon$ and $^{18}\epsilon$; DiFiore et al., 2010; Sigman et
263 al., 2009a,b; Granger et al., 2004, 2010). The high whole water column slope values for
264 $\delta^{18}\text{O}$ are in part due to the low $\delta^{18}\text{O}$ values (<2‰) of deep waters (LCDW and bottom
265 waters) underlying UCDW (Figure 2c). Although $\delta^{18}\text{O}$ slope values for the upper 250m
266 (Figure 4) tend to be smaller than whole water column slopes, they still clearly exceed
267 those for $\delta^{15}\text{N}_{\text{NO}_3}$.

268 The larger slope values of $\delta^{18}\text{O}$ vs. $\text{LN}[\text{NO}_3^-]$ regressions compared to those for $\delta^{15}\text{N}$, at
269 first sight might reflect the fact that the apparent discrimination factors for $^{18}\text{O}/^{16}\text{O}$
270 and $^{15}\text{N}/^{14}\text{N}$ ($^{15}\epsilon$; $^{18}\epsilon$) are not similar, as is expected ($\epsilon^{15} / \epsilon^{18} = 1$) in case nitrate uptake
271 (and also denitrification, but this is irrelevant for the oxygen-rich environment studied
272 here) is the sole process inducing isotopic fractionation (Granger et al., 2004, 2008;
273 Sigman et al., 2009b). The likeliness that nitrification in subsurface waters as well as in
274 the upper mixed layer is responsible for these observations is developed further
275 below. A further process that could divert the $\epsilon^{15} / \epsilon^{18}$ ratio from unity is diazotrophy,

276 evidence of which is discussed by Gonzalez et al. (2014). Dinitrogen fixation would
277 lower nitrate $\delta^{15}\text{N}$ without affecting $\delta^{18}\text{O}$. N_2 fixation rates for the upper 50 m for the
278 Plateau and R-2 sites do reach at most $0.2 \text{ mmol m}^{-2} \text{ d}^{-1}$ (Gonzalez et al., 2014). For the
279 Plateau site this represents only about 1% of the calculated best fit nitrification rate
280 (see later below) of $18 \text{ mmol m}^{-2} \text{ d}^{-1}$. No N_2 fixation rates are available for the Meander
281 sites, but assuming that the rate observed at Plateau and R-2 also applies for the
282 Meander site, N_2 fixation rate for the Meander would represent some 20% of the
283 calculated best-fit nitrification rate ($1 \text{ mmol m}^{-2} \text{ d}^{-1}$; see further below), which is a
284 significant fraction. For the Meander site, however, the nitrification rate itself is poorly
285 constrained (see below), making it difficult to definitively conclude here on the relative
286 significance of N_2 fixation and nitrification for that site.

287

288 *4.2 Differential behavior of $\delta^{15}\text{N}_{\text{NO}_3}$ and $\delta^{18}\text{O}_{\text{NO}_3}$ evidenced from $\Delta(15-18)$*

289 Differences between the $\delta^{15}\text{N}_{\text{NO}_3}$ and $\delta^{18}\text{O}_{\text{NO}_3}$ profiles are highlighted even more when
290 plotting the difference between these isotopic compositions (i.e., $\delta^{15}\text{N}_{\text{NO}_3} - \delta^{18}\text{O}_{\text{NO}_3} =$
291 $\Delta(15-18)$); see Figure 2d:). A striking feature that appears from the present data set are
292 the consistently low $\Delta(15-18)$ values ($<3\text{‰}$; range 0.8 - 3) in the upper 250 m for all 3
293 areas, reflecting the proportionally stronger enrichment of nitrate in ^{18}O than ^{15}N .

294 Note that the sole effect of nitrate uptake with similar $^{15}\text{N}/^{14}\text{N}$, $^{18}\text{O}/^{16}\text{O}$ discrimination
295 would have left $\Delta(15-18)$ unchanged (Sigman et al., 2005), which is not the case here.
296 Such a feature of low $\Delta(15-18)$ values ($<3\text{‰}$) throughout the surface layer where
297 nitrate concentrations are mostly $\geq 20 \text{ }\mu\text{M}$, appears characteristic not only for the
298 present spring data set, but also for the summer data obtained during KEOPS 1 (Trull et
299 al., 2008) and has not been reported for other Southern Ocean studies. Rafter et al.
300 (2013) report low values (2.5 - 3‰) in subsurface waters ($\sim 100 - 400 \text{ m}$; $<25 \mu\text{M NO}_3^-$)
301 at latitudes around 50°S but these are overlaid with surface waters ($<15 \mu\text{M NO}_3^-$) that
302 have high $\delta^{15}\text{N}_{\text{NO}_3}$ and $\delta^{18}\text{O}_{\text{NO}_3}$ values and $\Delta(15-18)$ values of about 3‰ (see their Fig.
303 4). The latter authors describe the low subsurface $\Delta(15-18)$ values (2.5 - 3‰), as being

304 the result of partial consumption of available nitrate in surface waters, export of low
305 $\delta^{15}\text{N-PN}$, and remineralisation - nitrification there. Since nitrate N, O cycles are
306 uncoupled and ambient seawater with a $\delta^{18}\text{O}$ close to zero (Archambeau et al., 1998) is
307 the main source of oxygen for this 'recycled' nitrate (Sigman et al., 2009b), the latter is
308 relatively more depleted in heavy ^{15}N isotope than in heavy ^{18}O isotope, and this
309 results in $\Delta(15-18)$ values $< 3\text{‰}$, as discussed by Rafter et al. (2013). However, as
310 stated above, in contrast to the results reported by the latter authors for Open
311 Antarctic Zone and Polar Front Zone surface waters (Pacific sector) we observe that
312 the subsurface trend of lowered $\Delta(15-18)$ continues in the upper mixed layer, reaching
313 values as low as 1‰ . We note that the lower $\Delta(15-18)$ values in the upper 200m
314 coincide with higher ammonium and nitrite contents (Figure 5), possibly reflecting
315 effects of nitrification, which could be either a local or imported condition (see section
316 4.5 below).

317 For the waters between 250 and 1250m (upper mesopelagic), which include the
318 UCDW, a number of $\Delta(15-18)$ data points are slightly in excess of 3‰ (Figure 2d) due
319 to low $\delta^{18}\text{O}_{\text{NO}_3}$ values (Figures 2d and 3). From Figure 3 it appears that this feature
320 concerns mainly stations at the Polar Front east of 74°E (stations TEW7; TEW8, F-L)
321 underlying high chlorophyll surface waters (Figure 1), as well as some sites closer to
322 the Kerguelen margin in the West, around 72°E (stations E4W; E5) (Figure 3). The
323 vertical $\delta^{18}\text{O}_{\text{NO}_3}$ profiles for these stations show deep $\delta^{18}\text{O}_{\text{NO}_3}$ values close to 1.65‰
324 (i.e., some 0.35‰ lower than the average deep ocean value of 2‰) (Figure 5). On the
325 other hand stations in the low chlorophyll central part of the PF meander (TEW5;
326 TEW6; E4-E; TNS6; E1), and also north of the PF (TNS1) and away from the Kerguelen
327 bloom (R-2), show mesopelagic $\delta^{18}\text{O}_{\text{NO}_3}$ values close to the deep ocean reference value
328 of 2‰ . So the question arises what particular process or condition can account for
329 these variations in mesopelagic $\delta^{18}\text{O}_{\text{NO}_3}$ values.

330 A simple calculation shows that the lowered $\delta^{18}\text{O}_{\text{NO}_3}$ values cannot be explained by
331 mesopelagic remineralisation and nitrification of organic N exported over the course of
332 a single production season. For the latter process to increase deep ocean nitrate

333 concentrations (taken as 31 μM) to the mesopelagic average value of 34.5 μM and to
334 decrease $\delta^{18}\text{O}_{\text{NO}_3}$ from the deep ocean value of 2‰ to 1.65‰ taking a $\delta^{18}\text{O}_{\text{water}}$ of -
335 0.4‰ (Archambeau et al., 1998) and $\delta^{18}\text{O}_{\text{NO}_3}$ of nitrification = 1.1‰ (Sigman et al.,
336 2009b), would require an export and complete remineralisation and nitrification of
337 organic nitrogen in the 250 to 1250m water column layer of some 20 to 100 mmol m^{-2}
338 d^{-1} to fit the observed $[\text{NO}_3^-]$ and $\delta^{18}\text{O}_{\text{NO}_3}$, respectively. This is about 10 to 50 times
339 larger than the export flux from the 150 m depth horizon estimated via the ^{234}Th -
340 deficit approach (average PN flux = 1.9 $\text{mmol m}^{-2} \text{d}^{-1}$; Planchon et al., 2014). We
341 speculate that the complex recirculation pattern generated by the basin topography
342 and the presence of the PF induces a multiple season integrative effect on the nitrate
343 isotopic signature of the deep water in the gyre structure. The presence of low $\delta^{18}\text{O}_{\text{NO}_3}$
344 values also at some stations located more to the West (72°E; Figure 3) is in agreement
345 with a scenario whereby the low mesopelagic $\delta^{18}\text{O}_{\text{NO}_3}$ signature at the Polar Front is
346 entrained with the cyclonic circulation of the PF meander. This signal transfer could be
347 quite fast considering that shipboard measurements by Lowered Acoustic Doppler
348 Current Profiler revealed a strong eastward current along the northern edge of the
349 basin as associated with a cyclonic circulation. This current stretches over the whole
350 water column and reaches a velocity of 25 cm s^{-1} (Y.H. Park; pers. communic., 2011).
351 Alternatively we could argue that the low $\delta^{18}\text{O}_{\text{NO}_3}$ feature is imported from elsewhere.
352 The mesopelagic waters in the 250 to 1250 m range do comprise UCDW waters (i.e.,
353 temperature maximum waters above the salinity maximum waters). As discussed by
354 Rafter et al., (2013) these waters carry heavy $\delta^{15}\text{N}_{\text{NO}_3}$ and decreased $\delta^{18}\text{O}_{\text{NO}_3}$ isotopic
355 signatures acquired at lower latitudes and resulting from a combination of processes
356 including: (i) partial nitrate assimilation in the surface waters feeding northward
357 flowing Antarctic Mode and Intermediate Waters, (Sigman et al., 2009b); (2) flux of
358 partially denitrified waters into surface waters (mainly in the Pacific and Indian oceans)
359 combined with nearly complete consumption of nitrate in the low latitude ocean,
360 yielding high $\delta^{15}\text{N}$ values for sinking PN (see Sigman et al., 2009a; Rafter et al., 2013).
361 This yields subtropical subsurface waters with high $\delta^{15}\text{N}_{\text{NO}_3}$ and low $\delta^{18}\text{O}_{\text{NO}_3}$, and thus
362 high $\Delta(15-18)$ values. These isotopic signatures are again advected southward with

363 deep water and become subsequently incorporated in CDW to join the circumpolar
364 circulation (Rafter et al., 2013) explaining the presence of $\Delta(15-18)$ values exceeding
365 3‰. In the Open Antarctic Zone, CDW upwells and its UCDW branch flows northward
366 to subduct at the Polar Front as SAMW and AAIW (Rafter et al., 2013).

367

368 4.3 Low $\delta^{15}\text{N}_{\text{NO}_3}$ values in bottom waters

369 The low $\delta^{15}\text{N}_{\text{NO}_3}$ values in the cold (~ 0.5 °C) bottom waters in vicinity of the Polar Front
370 (Figure 3) may possibly be brought about in case partial nitrification takes place in the
371 sediments and feeds isotopically light nitrate to the bottom waters, as has been
372 described for the Bering Sea Shelf by Granger et al. (2011). However, if such a process
373 is also operating here in the Kerguelen area, we would expect to see the effects more
374 marked in waters hugging the slopes surrounding the basin. Indeed, there is some
375 evidence for isotopically light NO_3^- in the western part of the W-E section (Figure 3),
376 but clearly, the strongest depletions do occur in waters close to, and underlying, the
377 Polar Front in the eastern part of the W-E section and which are quite remote from the
378 slope regions of the basin. These cold bottom waters are likely of southerly origin,
379 associated with the Fawn Trough Current which transports cold Antarctic waters of
380 eastern Enderby origin (Park et al., 2008) and possibly also partly with Deep Western
381 Boundary Current which is part of the deep cyclonic gyre in the Australian – Antarctic
382 Basin (McCartney and Donohue, 2007; Fukamachi et al., 2010). However, values
383 reported for the Polar Antarctic Zone in the Indian and Australian sectors do not show
384 evidence of deep ocean $\delta^{15}\text{N}_{\text{NO}_3}$ values lower than 5‰ (DiFiore et al., 2009). So it
385 remains uncertain where these low $\delta^{15}\text{N}_{\text{NO}_3}$ signatures in bottom waters underlying the
386 Polar Front area at 74-75°E originate from.

387

388 In the next sections we focus on the conditions in the upper 250m of water column
389 where our observations provide evidence of significant nitrification.

390

391 4.4 Co-variation of $\delta^{15}\text{N}_{\text{NO}_3}$ - $\delta^{18}\text{O}_{\text{NO}_3}$

392 Figure 8 shows the regressions of $\delta^{18}\text{O}_{\text{NO}_3}$ vs. $\delta^{15}\text{N}_{\text{NO}_3}$ for the Plateau, Meander and PF
393 areas. As expected from the discussions above, the regression slopes for whole water
394 column are larger than 1 (they vary between 1.4 and 1.5, for PF and Plateau areas,
395 respectively). The black line in Figure 8 reflects the expected regression in case
396 discrimination during nitrate uptake is similar for $^{18}\text{O}/^{16}\text{O}$ and $^{15}\text{N}/^{14}\text{N}$ and acts upon a
397 nitrate source reservoir that has a deep water isotopic signature (i.e., $\delta^{15}\text{N}_{\text{NO}_3} = 5\text{‰}$
398 and $\delta^{18}\text{O}_{\text{NO}_3} = 2\text{‰}$). When focusing on the upper 250m we note that slope values
399 decrease and come close to 1 for the PF area (slope = 1.14), while they are close to 1.3
400 for Plateau and Meander sites (Figure 8). For all 3 areas, it is clear, however, that data
401 points mostly fall above the expected regression. This condition is also clearly reflected
402 in the $\Delta(15-18)$ values which on average fall below 2.5‰ for the upper 200m of water
403 column (see Figure 2).

404 Figure 8 also shows the summer data obtained during KEOPS 1 (Trull et al., 2008)
405 superposed on the present KEOPS 2 spring data. This comparison is limited to the
406 upper 250 m of the water column, i.e. the depth range analysed during KEOPS 1 (Trull
407 et al., 2008). The summer data overlap tightly with the spring data but also sit above
408 the 1:1 line, defined above, but in contrast to spring, summer shows a slope value
409 close to 1 (0.98). However, a closer look reveals that the deep summer samples have
410 slightly more elevated $\delta^{18}\text{O}_{\text{NO}_3}$ values, tilting the regression and thereby decreasing the
411 slope value. These more elevated subsurface $\delta^{18}\text{O}_{\text{NO}_3}$ values may reflect the effect of
412 subsurface nitrification in an area of partial surface nitrate assimilation (Rafter et al.,
413 2013; Sigman et al. 2009b). When focusing on the mixed layer depth, the slopes of the
414 $\delta^{18}\text{O}_{\text{NO}_3}$ vs. $\delta^{15}\text{N}_{\text{NO}_3}$ regressions become even steeper for the Plateau (up to 1.65) and
415 Meander areas and for the KEOPS 1 data set (Figure 8), but not for the PF area. Thus,
416 within the upper 250m and even more so in the upper mixed layer, the variations of
417 $\delta^{18}\text{O}_{\text{NO}_3}$ values clearly exceed those for corresponding $\delta^{15}\text{N}_{\text{NO}_3}$ values. Such a condition
418 may result from the remineralisation – nitrification organic nitrogen (Sigman et
419 al. 2009b, DiFiore et al., 2009). Also, the absence of a clear differentiation between

420 summer (KEOPS 1) and spring (KEOPS 2) conditions (Figure 8; we would expect to see
421 the summer condition further up the line with higher $\delta^{15}\text{N}$ and $\delta^{18}\text{O}$ values) is quite
422 puzzling, and may reflect the fact that the nitrate consumed is being largely
423 replenished from remineralisation coupled to nitrification, thereby dampening the
424 enrichment of ^{15}N due to uptake (but enhancing the ^{18}O enrichment). We also note
425 that the average deficit of silicic acid and nitrate in the mixed layer vs. the winter
426 values in underlying T_{\min} waters are systematically $\gg 1$ (up to 4) for the whole area,
427 while $\text{Si}(\text{OH})_4/\text{NO}_3^-$ uptake ratios are generally close to 1 (0.74 to 1.51) for the Plateau
428 and Meander areas, consistent with iron replete conditions there (Closset et al., 2014;
429 Cavagna et al., 2014). The larger deficit of silicic acid compared to nitrate could thus
430 partly result from shallow recycling of nitrogen. . In fact nitrate contents stay relatively
431 high throughout the growth season and KEOPS 1 summer nitrate values remain
432 generally in excess of 20 μM (Trull et al., 2008), while summer silicic acid
433 concentrations run low to near depletion, despite the $\text{Si}(\text{OH})_4/\text{NO}_3^-$ uptake ratio being
434 close to 1 (Mosseri et al., 2008). This is further evidence for significant nitrification in
435 the upper mixed layer. The combined effect of nitrate uptake and nitrification in the
436 euphotic zone will result in decoupling the $\delta^{15}\text{N}_{\text{NO}_3}$ and $\delta^{18}\text{O}_{\text{NO}_3}$ signals, thereby
437 decreasing their average deep ocean difference of 3‰.

438 The question can be raised to what extent this is a local or imported condition from an
439 upstream area. At the HNLC reference station, located upstream of the Kerguelen
440 Plateau and Meander areas the upper mixed layer values of $\delta^{15}\text{N}$ and $\delta^{18}\text{O}$ are
441 increased by about 1.2‰ and 2‰, respectively, relative to local deep waters (Figure
442 2). This results in decreased $\Delta(15-18)$ values (average value upper 100m = 2.25‰),
443 which are similar to values for the Meander ($\Delta(15-18) = 2.20 \pm 0.42\%$), PF ($\Delta(15-18) =$
444 $2.39 \pm 0.28\%$) and also Plateau sites sampled during the earlier part of the study
445 period (A3-1; E4W-1; TNS8; TEW4; E4W1; $\Delta(15-18) = 2.47 \pm 0.26\%$). Such values,
446 however, are larger than those for Plateau sites sampled toward the end of the study
447 period (E4W2 and A3-2; average $\Delta(15-18) = 1.79 \pm 0.25\%$), adding evidence for
448 ongoing nitrification during this early bloom phase, at least above the Plateau.

449 Meander and Polar Front sites on the contrary do not show such evidence as their
450 upper ocean $\Delta(15-18)$ values do not differentiate from the value at the HNLC reference
451 station.

452 Nitrification could possibly occur at the shelf sediment water column interface, as
453 reported for the low nitrate Bering Sea shelf, characterized by high NH_4^+ levels
454 (Granger et al., 2011; 2013). For instance, at the shallow (< 100m) TEW1 shelf station
455 (see Figure 6A) ammonium contents are enhanced (up to 1.1 μM) close to the seafloor.
456 We note, however, that $\Delta(15-18)$ values are relatively large, averaging 2.3‰ (Figure
457 6A; Table A1), a condition that is not indicative of significant nitrification. Furthermore
458 the shallow TEW1 station is located north of the Polar Front, and surface waters
459 advected from this shallow shelf area flow north, north-east, staying north of the PF
460 (see surface water flow lines in Figure 1), away from A3. Except for this station TEW1
461 we do not see evidence for nitrification at the site sediment water column boundary
462 layer elsewhere above the Kerguelen Plateau, though we have no data for the shallow
463 water column (<100m) close to Heard Island located further south on the Plateau,
464 some 400 Km upstream of site A3 (Figure 1a). During KEOPS 1 (summer 2005) NH_4^+ and
465 NO_2^- concentrations at the C1 site close to Heard Island reached up to 0.7 and 0.4 μM ,
466 respectively and a single nitrate isotopic measurement for the C1 site gave a $\Delta(15-18)$
467 value of 2.13‰ (Trull et al., 2008) so conditions similar to those observed here for site
468 TEW1. Especially the large $\Delta(15-18)$ values (>2‰) observed for these two shallow
469 (<100m) plateau sites make it unlikely that sediment boundary layer nitrification is a
470 source of nitrate to the mixed layer above the main Kerguelen Plateau area south of
471 the Polar Front. In the next section we evaluate the strength of a possible nitrification
472 in the surface layers.

473

474 *4.5 Calculating the temporal evolution of $\delta^{15}\text{N}_{\text{NO}_3}$ and $\delta^{18}\text{O}_{\text{NO}_3}$ in the surface mixed*
475 *layer*

476 The similarity of the ranges of upper ocean nitrate isotopic compositions during early
477 (KEOPS 1) and late (KEOPS 2) season (Figure 8) raises the question whether the
478 Kerguelen system had already reached some steady state condition for nitrogen
479 cycling early in the season, with nitrate consumption being mostly balanced by
480 remineralization combined with nitrification. However, earlier studies, suggest that the
481 evidence for significant euphotic zone nitrification in Southern Ocean surface waters is
482 weak (Olson, 1981; Bianchi et al., 1997; Trull et al., 2008; DiFiore et al., 2009). To
483 resolve this apparent controversy we will estimate the strength of nitrification in the
484 upper mixed layer. We apply a mass balance approach for both, $\delta^{15}\text{N}_{\text{NO}_3}$ and $\delta^{18}\text{O}_{\text{NO}_3}$ in
485 the mixed layer of Plateau and Meander stations where data on temporal evolution
486 are available. We take advantage of the fact that nitrate and ammonium uptake rates
487 were measured during KEOPS 2 (Cavagna et al., 2014) and also that values of isotopic
488 composition of suspended and sinking material are available (Trull et al., 2014;
489 Dehairs, unpublished results) Note that the model calculations presented here cover a
490 limited length of growth period (about one month). More complex model calculations
491 describing the evolution nitrification over the full growth season are presented
492 elsewhere (Fripiat et al., submitted).

493 We take the upper 100 m nitrate conditions observed during the earliest visit to the
494 Plateau and Meander as the initial conditions (i.e. conditions for stations A3-1 and
495 TNS6, respectively). Euphotic zone (0.01% PAR; 57 to 137m deep) integrated nitrate
496 uptake rates reported by Cavagna et al. (2014) do show an increase by some 30% for
497 the Meander region (Stations E1, E3, E4-E and E5; 27 day period). For the Plateau
498 region only two N-uptake profiles (stations E4-W; A3-2) were measured, apart by just 4
499 days. Nitrate uptake for the Meander sites are on average $12.4 \pm 2.2 \text{ mmol m}^{-2} \text{ d}^{-1}$ ($n =$
500 4) while for the Plateau sites they are 36 ± 4.7 ($n=2$). Ammonium uptake rates are 6.6
501 $\pm 1.4 \text{ mmol m}^{-2} \text{ d}^{-1}$ ($n=4$) and 6.2 ± 1.9 ($n=2$) for Meander and Plateau sites,
502 respectively. Using these average nitrate uptake rates we calculate the nitrate
503 concentrations (called residual nitrate) that would be present in the upper 100 m at
504 the end of the observation period in case uptake is the sole process affecting the

505 nitrate concentration. Nitrate concentrations at stations A3-1 (Plateau) and TNS6
 506 (Meander) were considered to represent the initial conditions, whereas concentrations
 507 at stations A3-2 (Plateau) and station E5 (Meander), visited 27 days after A3-1 and
 508 TNS6, respectively, represent the conditions at the end of the observation period.
 509 Residual nitrate values are slightly ($\Delta[\text{NO}_3^-] = 1.8 \mu\text{M} = 6\%$; Meander) to significantly
 510 lower ($\Delta[\text{NO}_3^-] = 4.1 \mu\text{M} = 25\%$; Plateau) than measured values (see Table 3). The
 511 isotopic composition of the residual nitrate is then calculated from the estimated
 512 fraction of nitrate remaining, using a discrimination of 5‰ for both $^{15}\text{N}/^{14}\text{N}$ and
 513 $^{18}\text{O}/^{16}\text{O}$ (Sigman et al., 1999; DiFiore et al., 2010) and considering that the surface
 514 mixed layer operates as a closed system (Rayleigh fractionation applies). The
 515 calculated isotopic compositions of the residual nitrate are heavier than the measured
 516 ones. The differences between calculated and observed isotopic values are: for $\delta^{15}\text{N}$
 517 0.22‰ and 1.45‰ and for $\delta^{18}\text{O}$, 0.10 and 0.98‰ for Meander and Plateau areas,
 518 respectively. For the Meander differences are small (close to the analytical precision)
 519 and so the calculated nitrification rate is poorly constrained. For the Plateau area the
 520 differences are larger and as a result calculated nitrification combined with nitrate
 521 upwelling are better constrained.

522 The isotope effects associated with nitrification are taken as follows, assuming a
 523 steady state between the production and consumption of both ammonium and nitrite
 524 (e.g., Fripiat et al., 2014):

525 For $\delta^{15}\text{N}_{\text{NO}_3}$: $\text{Nitrif.} [\delta^{15}\text{N}_{\text{PN}} - \epsilon_R + x (\epsilon_{\text{NH}_4\text{U}} - \epsilon_{\text{AMO}}) + y (\epsilon_{\text{NIU}} - \epsilon_{\text{NIO}})]$ (1)

526 For $\delta^{18}\text{O}_{\text{NO}_3}$: $\text{Nitrif.} (\delta^{18}\text{O}_{\text{H}_2\text{O}} + 1.1)$ (Sigman et al., 2009b) (2)

527 with Nitrif = the nitrification rate, $\delta^{15}\text{N}_{\text{PN}}$ = the N isotopic composition of suspended
 528 material (1.74‰); $\delta^{18}\text{O}_{\text{H}_2\text{O}}$ = the oxygen isotopic composition of ambient water; ϵ_R = the
 529 discrimination during remineralisation (2‰); $\epsilon_{\text{NH}_4\text{U}}$ = the isotope discrimination during
 530 NH_4^+ uptake (5‰); ϵ_{AMO} = the discrimination during NH_4^+ oxidation (15‰); ϵ_{NIU} = the
 531 discrimination during nitrite uptake (1‰); ϵ_{NIO} = the discrimination during nitrite
 532 oxidation (-12.5‰); x = the fractional yield of ammonium uptake relative to

533 ammonium remineralisation (with NH_4^+ remin. = AmU + AmO) and y = the fractional
 534 yield of nitrite uptake relative to ammonium oxidation (with AmO = NiU +
 535 NiO). Table 2 gives the selected values for the different discrimination factors as taken
 536 from the literature.

537 The theoretical in-situ nitrate isotopic values at the end of the observation period are
 538 considered to result from the weighted impact of uptake, nitrification and upwelling
 539 and were calculated as follows:

540 $\delta^{15}\text{N}_{\text{NO}_3} =$

541
$$\frac{\text{Uptake}(\delta^{15}\text{N}_{\text{NO}_3} - \varepsilon_{\text{NaU}} Lnf) + \text{Nitrif}[\delta^{15}\text{N}_{\text{PN}} - \varepsilon_R + x(\varepsilon_{\text{NH}_4\text{U}} - \varepsilon_{\text{AmO}}) + y(\varepsilon_{\text{NiU}} - \varepsilon_{\text{NiO}})] + \text{Upw}(\delta^{15}\text{N}_{\text{NO}_3\text{Tmin}})}{\text{Uptake} + \text{Nitrif} + \text{Upwelling}}$$

542

543 and

544
$$\delta^{18}\text{O}_{\text{NO}_3} = \frac{\text{Uptake}(\delta^{18}\text{O}_{\text{NO}_3} - \varepsilon_{\text{NaU}} Lnf) + \text{Nitrif}(\delta^{18}\text{O}_{\text{H}_2\text{O}}) + \text{Upw}(\delta^{18}\text{O}_{\text{NO}_3\text{Tmin}})}{\text{Uptake} + \text{Nitrif} + \text{Upwelling}}$$

545

546 With the different ε values = the isotopic discriminations; $\delta^{15}\text{N}_{\text{NO}_3\text{Tmin}}$ and $\delta^{18}\text{O}_{\text{NO}_3\text{Tmin}}$ =
 547 isotopic composition for the subsurface temperature minimum waters (ε and δ values
 548 are given in Table 2); f = fraction of remaining nitrate; x and y , as defined above;
 549 Uptake = nitrate uptake rate; Nitrif = nitrification rate; Upw = rate of vertical advection
 550 of nitrate.

551 The best fit between observed and calculated isotopic compositions is searched using a
 552 optimization scheme with nitrification, upwelling from subsurface waters (T_{min} waters
 553 at 100 to 150 m depth), NH_4^+ oxidation and NO_2^- uptake as adjustable variables.

554 The matching of observed and calculated nitrate draw down and the matching of NH_4^+
 555 oxidation with NO_2^- uptake + nitrification are imposed constraints. The best fit
 556 calculations yield nitrification rates of 1.7 ± 2.3 and 17.4 ± 4.1 $\text{mmol m}^{-2} \text{d}^{-1}$ for
 557 Meander and Plateau, respectively (Table 3). Best fit values are 0 and $5.5 \text{ mmol m}^{-2} \text{d}^{-1}$

558 for NO_2^- uptake and 4.0 and 6.1 $\text{mmol m}^{-2} \text{d}^{-1}$ for NO_3^- upwelling, for Meander and
559 Plateau sites respectively (Table 3). We note that the values for nitrate upwelling are
560 quite similar to the value of 7.4 $\text{mmol m}^{-2} \text{d}^{-1}$ we calculate, as based on an Ekman
561 pumping velocity of $3 \times 10^{-6} \text{ m s}^{-1}$ for the studied KEOPS 2 area, reported by Gille et al.
562 (2014), and an average subsurface (150m) NO_3^- concentration of 28.5 μM . In case the
563 NO_3^- upwelling rate is fixed and set equal to the calculated value of 7.4 $\text{mmol m}^{-2} \text{d}^{-1}$
564 based on the Ekman pumping velocity, the best fit nitrification rates are slightly smaller
565 but more constrained with values of 1.3 ± 1.2 and $16.2 \pm 2.4 \text{ mmol m}^{-2} \text{d}^{-1}$, for
566 Meander and Plateau, respectively. For the Meander site the evidence for nitrification
567 is poor, in agreement with the fact that surface water $\Delta(15-18)$ values remain small
568 and quite constant over the 1 month period of observation and are similar to those for
569 the HNLC R-2 reference station. We also verified the effect of nitrite presence on these
570 calculations. Indeed, Rafter et al. (2012) report a lowering of the true nitrate $\delta^{15}\text{N}$ and
571 $\delta^{18}\text{O}$ compositions by 0.4‰ and 0.2‰, respectively, in case nitrite contents amount to
572 some 0.8% of the nitrate content, what is the case here (see also methods section 2.2).
573 It appears that nitrification rates above the Plateau would be reduced by at most 7%
574 due to unaccounted for nitrite.

575 We performed a sensitivity test to verify the range (minimum – maximum) of
576 nitrification, nitrite uptake and nitrate upwelling rates, taking into account the
577 measurement errors on isotopic compositions (as given in the Methods section) and
578 the observed variability on nitrate and ammonium uptake rates. It appears for the
579 Meander site that the min. – max. range of possible nitrification rates reaches from 0
580 to 11 $\text{mmol m}^{-2} \text{d}^{-1}$, a range which narrows from 0 to 4 $\text{mmol m}^{-2} \text{d}^{-1}$ in case NO_3^-
581 upwelling is kept fixed. The situation is quite different for the Plateau site where the
582 min. – max. range of nitrification reaches from 6 to 27 $\text{mmol m}^{-2} \text{d}^{-1}$ which narrows
583 down from 10 to 22 $\text{mmol m}^{-2} \text{d}^{-1}$ when upwelling is kept fixed. From this we conclude
584 for the Plateau area significant surface layer nitrification needs to be invoked to
585 explain the observed nitrate isotopic compositions and which may represent as much
586 as 48% of the nitrate uptake. For the Meander the evidence for nitrification is poor.

587 The conditions leading to the high upper ocean nitrification above the Plateau are
588 believed to be related with the depth range of the euphotic layer and the mixed layer.
589 Above the Plateau the euphotic layer (0.1% PAR level) is consistently shallower than
590 the mixed layer and any nitrate produced from nitrification, a process which is
591 supposedly inhibited by light (Olson, 1981; Guerero and Jones, 1996), at the bottom of
592 the euphotic layer therefore becomes retained in the surface mixed layer. This aspect
593 is discussed in more detail in a paper by Fripiat et al. (submitted). The calculated
594 nitrification rate for the Kerguelen Plateau significantly exceeds some earlier estimates
595 and which led to the conclusion that nitrification is a rather minor process which
596 accounts for <10% of phytoplankton nitrate uptake in Southern Ocean waters (Olson,
597 1981; Trull et al., 2008; DiFiore et al., 2009). In contrast, high nitrification rates
598 reaching levels similar to the phytoplankton nitrate demand appear to be common for
599 oligotrophic systems (see e.g., Yool et al., 2007; Wankel et al., 2007; Mulholland and
600 Lomas, 2008 and references therein). Nevertheless, conditions for significant
601 nitrification activity appear to be met in the studied Kerguelen area. For one thing,
602 ammonium concentrations are relatively high, reaching up to 0.5, 0.7 and 0.8 μM
603 within the first 100m for the PF, Meander and Plateau sites, respectively (Figure 3)
604 thus providing the substrate for any bacterial and archaeal ammonium oxidizing
605 activity. Furthermore, nitrite concentrations reach up to 0.33 μM in the upper 100m of
606 water column (Table 1), again indicating nitrification activity is ongoing there. Archaea
607 do abound in the Southern Ocean (Church et al., 2003) and may exhibit a specific
608 affinity for ammonia similar to the one for diatoms, as reported for the cultivated
609 marine ammonia oxidizing archeon (*Nitrosopumilus maritimus*) (Martens-Habbena et
610 al., 2009 and Stahl and de la Torre, 2012).

611

612 Conclusions

613 The present data set adds to the existing data set on dual nitrate isotopic composition
614 for the seasonally ice covered Polar Antarctic Zone (DiFiore et al., 2009) and a
615 meridional section in the Pacific sector (Rafter et al., 2013). It also adds information on

616 the seasonal evolution of nitrate isotopic composition in the iron fertilized Kerguelen
617 area, by complementing an earlier study that was conducted during summer in the
618 same area (Trull et al., 2008). Published work related to the late summer KEOPS 1
619 study in the same area as investigated in the present study, highlighted the large
620 difference between the seasonal drawdown of silicic acid and nitrate, with the latter
621 being moderate despite similar Si, N uptake rates (Mosseri et al., 2008). Those results
622 pointed toward the occurrence of significant remineralisation and nitrate production.
623 The present work confirms the significance of nitrification in the area, with nitrification
624 representing some 47% of the nitrate uptake over the Kerguelen Plateau area. This
625 finding of large nitrification rates in nitrate-replete environments was unexpected a
626 priori, in view of the earlier studies outside the Kerguelen area which concluded to
627 minor nitrification effects in Southern Ocean surface waters (Olson, 1981, DiFiore et
628 al., 2009). A direct result of this condition is that estimates of New or Exportable
629 Production which are based on the assumption that all surface water nitrate results
630 from nitrification in the deep ocean and vertical supply to the surface waters, are too
631 high. Correcting New Production for the effect of nitrification would bring closer the
632 estimates of exportable production and Export production during KEOPS 2, as
633 measured with the ²³⁴Th methodology (see papers by Cavagna et al., 2014 and
634 Planchon et al., 2014, both in this issue).

635

636

637

638 Acknowledgements

639 We thank the Captain and the crew of Marion-Dufresne as well as KEOPS 2 Chief
640 scientists B. Quéguiner and S. Blain for their assistance and help during the cruise. We
641 are grateful to the Institut Paul Emile Victor (IPEV) for having granted us access to the
642 Marion Dufresne facilities. This work was supported by the French Research program
643 of INSU-CNRS LEFE-CYBER the French ANR(SIMI-6 program, ANR-10-BLAN-0614), the
644 French CNES (Centre National d'Etudes Spatiales) and the French Polar Institute IPEV
645 (Institut Polaire Paul-Emile Victor). The research was conducted with grants from
646 Belgian Science Policy (BELSPO, grant SD/CA/05A); Flanders Research Foundation
647 (FWO; grant G071512N); Vrije Universiteit Brussel, Strategic Research Plan); the
648 Antarctic Climate and Ecosystem Cooperative Research Center (ACE-CRC, Hobart,
649 Australia). The altimeter and colour/temperature products for the Kerguelen area
650 were produced by Ssalto/Duacs and CLS with support from Cnes. F. Fripiat is Post-Doc
651 at FWO, Flanders Research Foundation; C. Fernandez was partially supported by
652 Fondap 15110027 Incar. We acknowledge the help of Natacha Brion, Leen Rymenans
653 and Michael Korntheuer during nitrate and nitrate isotope analyses and thank the two
654 anonymous reviewers for their constructive comments and criticisms.

655

656

657

658 References:

659 Archambeau, A.-S., Pierre, C., Poisson, A., and Schauer, B.: Distributions of oxygen and
660 carbon stable isotopes and CFC-12 in the water masses of the Southern Ocean at
661 30°E from South Africa to Antarctica: results of the CIVA1 cruise, *J. Mar. Syst.*, 17,
662 25-38, 1998.

663 Bianchi, M., Feliatra, F., Tréguer, P., Vincendeau, M.-A., and Morvan, J.: Nitrification
664 rates, ammonium and nitrate distribution in upper layers of the water column and
665 in sediments of the Indian sector of the Southern Ocean, *Deep-Sea Res. Pt. II*, 44,
666 1017-1032, 1997.

667 Blain, S., Capparos, J., Guéneuguès, A., Obernosterer, I., and Oriol, L.: Distributions and
668 stoichiometry of dissolved nitrogen and phosphorus in the iron fertilized region
669 near Kerguelen (Southern Ocean), *Biogeosciences Discuss.*, 11, 9949-9977.
670 doi:10.5194/bgd-11-9949-2014, 2014.

671 Blain, S., Quéguiner, B., Armand, L., Belviso, S., Bombled, B., Bopp, L., Bowie, A.,
672 Brunet, C., Brussaard, C., Carlotti, F., Christaki, U., Corbière, A., Durand, I.,
673 Ebersbach, F., Fuda, J.-L., Garcia, N., Gerringa, L., Griffiths, B., Guigue, C., Guillerm,
674 C., Jacquet, S., Jeandel, C., Laan, P., Lefèvre, D., Lo Monaco, C., Malits, A., Mosseri,
675 J., Obernosterer, L., Park, Y.-H., Picheral, M., Pondaven, P., Remenyi, T., Sandroni, V.,
676 Sarthou, G., Savoye, N., Scouarnec, L., Souhaut, M., Thuiller, D., Timmermans, K.,
677 Trull, T., Uitz, J., van Beek, P., Veldhuis, M., Vincent, D., Viollier, E., Vong, L., and
678 Wagener, T.: Effect of natural iron fertilization on carbon sequestration in the
679 Southern Ocean, *Nature*, 446, 1070-1074, 2007.

680 Blain, S., Quéguiner, B., and Trull, T.: The natural iron fertilization experiment KEOPS
681 (Kerguelen Ocean and Plateau compared Study): An overview, *Deep-Sea Res. Pt. II*,
682 55, 559-565, 2008.

683 Böhlke, J., Mroczkowski, S., and Coplen, T.B.: Oxygen isotopes in nitrate: New
684 reference materials for ^{18}O : ^{17}O : ^{16}O measurements and observations on nitrate-
685 water equilibrations, *Rapid Comm. Mass Sp.*, 17, 1835-1846, 2003.

686 Buchwald, C., and Casciotti, K.L.: Oxygen isotopic fractionation and exchange during
687 bacterial nitrite oxidation, *Limnol. Oceanogr.*, 55, 1064-1074, 2010.

688 Casciotti, K.L.: Inverse kinetic isotope fractionation during bacterial nitrite oxidation,
689 *Geochim. Cosmochim. Acta*, 73, 2061-2076, 2009.

690 Casciotti, K.L., Böhlke, J.K., McIlvin, M.R., Mroczkowski, S.J. and Hannon, J.E.: Oxygen
691 Isotopes in Nitrite: Analysis, Calibration, and Equilibration, *Anal. Chem.*, 79, 2427-
692 2436, 2007.

693 Casciotti, K.L., Sigman, D.M., Hastings, M. G., Böhlke, J.K., and Hilkert, A.:
694 Measurement of the oxygen isotopic composition of nitrate in seawater and
695 freshwater using the denitrifier method, *Anal. Chem.*, 74, 4905-4912, 2002.

696 Casciotti, K.L., Sigman, D.M., and Ward, B.B.: Linking diversity and stable isotope
697 fractionation in ammonia-oxidizing bacteria, *Geomicrobiol. J.*, 20, 335-353, 2003.

698 Cavagna, A.J., Lefèvre, D., Dehairs, F., Elskens, M., Fripiat, F., Closset, I., Lasbleiz, M.,
699 Flores-Leive L., Cardinal, D., Leblanc, K., Fernandez, C., Oriol, L., Blain, S., and
700 Quéguiner, B.: Biological productivity regime in the surface water around the

701 Kerguelen Island in the Southern Ocean – from the use of an integrative approach,
702 Biogeosciences Discuss., 11, doi:10.5194/bgd-11-18073-2014, 2014.

703 Church, M.J., DeLong, E.F., Ducklow, H.W., Karner, M.B., Preston, C.M., and Karl, D.M.:
704 Abundance and distribution of planktonic Archaea and Bacteria in the waters west
705 of the Antarctic Peninsula, *Limnol. Oceanogr.*, 48, 1893-1902, 2003.

706 Closset, I., Lasbleiz, M., Leblanc, K., Quéguiner, B., Cavagna, A.-J., Elskens, M., Navez, J.,
707 and Cardinal, D.: Seasonal evolution of net and regenerated silica production
708 around a natural Fe-fertilized area in the Southern Ocean estimated from Si
709 isotopic approaches, *Biogeosciences*, 11, 5827–5846, doi:10.5194/bg-11-5827-
710 2014, 2014.

711 DiFiore, P.J., Sigman, D.M., and Dunbar, R.B.: Upper ocean nitrogen fluxes in the Polar
712 Antarctic Zone: constraints from the nitrogen and oxygen isotopes of nitrate,
713 *Geochem., Geophys. Geosyst.*, 10, doi:10.1029/2009GC002468, 2009.

714 DiFiore, P.J., Sigman, D.M., Karsh, K.L., Trull, T.W., Dunbar, R.B., and Robinson, R.S.:
715 Poleward decrease in the isotope effect of nitrate assimilation across the Southern
716 Ocean, *Geophys. Res. Lett.*, 37, L17601, doi:10.1029/2010GL044090, 2010.

717 DiFiore, P.J., Sigman, D.M., Trull, T.W., Lourey, M.J., Karsh, K., Cane, G., and Ho, R.:
718 Nitrogen isotope constraints on subantarctic biogeochemistry, *J. Geophys. Res.*,
719 111, C08016, doi:10.1029/2005JC003216, 2006.

720 Fogel, M.L., and Cifuentes, L.A.: Isotope fractionation during primary production, in:
721 *Organic Geochemistry*, edited by Engel, M.H., and Macko, S.A, Plenum Press, N.Y.,
722 73-98, 1993.

723 Fripiat, F., Sigman, D. M., Fawcett, S. E., Rafter, P. A., Weigand, M. A. and Tison, J.-L.:
724 New insights into sea ice nitrogen biogeochemical dynamics from the nitrogen
725 isotopes, *Global Biogeochem. Cy.*, 28, DOI: 10.1002/2013GB004729, 2014.

726 Fukamachi, Y., Rintoul, S. R., Church, J. A., Aoki, S., Sokolov, S., Rosenberg, M. A., and
727 Wakatsuchi, M.: Strong export of Antarctic bottom water east of the Kerguelen
728 Plateau, *Nat. Geosci.*, 3, 327–331, 2010.

729 Gille, S. T., Carranza, M. M., Cambra, R., and Morrow, R.: Wind-induced upwelling in
730 the Kerguelen Plateau Region, *Biogeosciences*, 11, 6389–6400,
731 2014doi:10.5194/bg-11-6389-2014, 2014.

732 Granger, J., Prokopenko, M.G., Mordy, C.W., and Sigman, D.M., The proportion of
733 remineralized nitrate on the ice-covered eastern Bering Sea shelf evidenced from
734 the oxygen isotope ratio of nitrate, *Global Biogeochem. Cy.*, 27, 962 – 971,
735 doi:10.1002/gbc.20075, 2013.

736 Granger, J., Prokopenko, M. G., Sigman, D. M., Mordy, C. W., Morse, Z. M., Morales, L.
737 V., Sambrotto, R. N., and Plessen, B.: Coupled nitrification-denitrification in
738 sediment of the eastern Bering Sea shelf to ¹⁵N enrichment of fixed N in shelf
739 waters, *J. Geophys. Res.*, 116, doi:10.1029/2010JC006751, 2011.

740 Granger, J., Sigman, D. M., Needoba, J. A., and Harrison, P. J.: Coupled nitrogen and
741 oxygen isotope fractionation of nitrate during assimilation by cultures of marine
742 phytoplankton, *Limnol. Oceanogr.*, 49, 1763–1773, 2004.

743 Granger, J., Sigman, D.M., Lehmann, M.F., and Tortell, P.D.: Nitrogen and oxygen
744 isotope fractionation during dissimilatory nitrate reduction by denitrifying bacteria,
745 *Limnol. Oceanogr.*, 53, 2533–2545, 2008.

746 Granger, J., Sigman, D. M., Rohde, M. M., Maldonado, M. T., and Tortell, P. D.: N and O
747 isotope effects during nitrate assimilation by unicellular prokaryotic and eukaryotic
748 plankton cultures, *Geochim. Cosmochim. Ac.*, 74, 1030–1040, 2010.

749 Guerrero, M. A., and Jones, R. D.: Photoinhibition of marine nitrifying bacteria 1.
750 Wavelength-dependent response, *Mar. Ecol. Prog. Ser.* 141, 183–192, 1996.

751 Hoch, M. P., Fogel, M. L., and Kirchman, D. L.: Isotope fractionation associated with
752 ammonium uptake by a marine bacterium, *Limnol. Oceanogr.*, 37, 1447–1459,
753 1992.

754 Jacquet, S. H. M., Dehairs, F., Savoye, N., Obernosterer, I., Christaki, U., Monnin, C.,
755 and Cardinal, D.: Mesopelagic organic carbon remineralization in the Kerguelen
756 Plateau region tracked by biogenic particulate Ba, *Deep-Sea Res. Pt. II*, 55, 868–
757 879, 2008.

758 Jacquet, S. H. M., Dehairs, F., Cavagna, A. J., Planchon, F., Monin, L., André, L., Closset,
759 I., and Cardinal, D.: Early season mesopelagic carbon remineralization and transfer
760 efficiency in the naturally iron-fertilized Kerguelen area, *Biogeosciences Discuss.*,
761 11, 9035–9069, 10doi:10.5194/bgd-11-9035-2014, 2014.

762 Kendall, C.: Tracing nitrogen sources and cycling in catchments, in: *Isotope Tracers in*
763 *Catchment Hydrology*, edited by: Kendall, C., and McDonnell, J. J., Elsevier, 519–
764 576, 1998.

765 Knapp, A.N., Sigman, D.M., Lipschultz, F., Kustka, A.B., and Capone, D.G.: Interbasin
766 isotopic correspondence between upper - ocean bulk DON and subsurface nitrate
767 and its implications for marine nitrogen cycling, *Global Biogeochem. Cy.*, 25,
768 GB4004, doi:10.1029/2010GB003878, 2011.

769 Lasbleiz, M., Leblanc, K., Blain, S., Ras, J., Cornet-Barthaux, V., Hélias Nunige, S.,
770 and Quéguiner, B.: Pigments, elemental composition (C, N, P, Si) and stoichiometry
771 of particulate matter, in the naturally iron fertilized region of Kerguelen in the
772 Southern Ocean, *Biogeosciences*, 11, 5931–5955, doi:10.5194/bg-11-5931-2014,
773 2014.

774 Martens-Habbena, W., Berube, P. M., Urakawa, H., de la Torre, J. R., and Sath, D. A.:
775 Ammonia oxidation kinetics determine niche separation of nitrifying Archaea and
776 Bacteria, *Nature*, 461, 976–979, 2009.

777 McCartney, M. S. and Donohue, K. A.: A deep cyclonic gyre in the Australian–Antarctic
778 Basin, *Prog. Oceanogr.*, 75, 675–750, 2007.

779 Möbius, J.: Isotope fractionation during nitrogen remineralization (ammonification):
780 Implications for nitrogen isotope biogeochemistry, *Geochim. Cosmochim. Ac.*, 105,
781 422-432, 2013.

782 Mosseri, J., Quéguiner, B., Armand, L., and Cornet-Barthaux, V.: Impact of iron on
783 silicon utilization by diatoms in the Southern Ocean: a case of Si/N cycle decoupling
784 in a naturally iron–enriched area, *Deep-Sea Res. Pt. II*, 55, 801–819, 2008.

785 Mulholland, M. R. and Lomas, M. W.: Nitrogen uptake and assimilation, in: *Nitrogen in*
786 *the Marine Environment*, edited by: Mulholland, M. R. and Capone, D. J., Elsevier,
787 303–384, 2008.

788 Olson, R. J.: N tracer studies of the primary nitrite maximum, *J. Mar. Res.*, 39, 203–226,
789 1981.

790 Olson, R. J.: Differential photoinhibition of marine nitrifying bacteria - a possible
791 mechanism for the formation of the primary nitrite maximum, *J. Mar. Res.*, 39,
792 227–238, 1981.

793 Park, Y.-H., Durand, I., Kestenare, E., Rougier, G., Zhou, M., d'Ovidio, F., Cottéa, C., and
794 Lee, J.-H.: Polar Front around the Kerguelen Islands: an up-to-date determination
795 and associated circulation of surface/subsurface waters, *J. Geophys. Res.–Oceans*,
796 119, DOI: 10.1002/2014JC010061, 2014.

797 Park, Y.-H., F. Roquet, I. Durand, and Fuda, J.-L.: Large-scale circulation over and
798 around the Northern Kerguelen Plateau, *Deep-Sea Res. Pt. II*, 55, 566–581, 2008.

799 Paul, D., Skrzypek, G., and Fórizs, I.: Normalization of measured stable isotopic
800 compositions to isotope reference scales – a review, *Rapid Commun. Mass Sp.*, 21,
801 3006–3014, 2007.

802 Pennock, J. R., Velinsky, D. J., Ludlam, J. M., and Sharp, J. H.: Isotopic fractionation of
803 ammonium and nitrate during uptake by *Skeletonema costatum*: implications for
804 $\delta^{15}\text{N}$ dynamics under bloom conditions, *Limnol. Oceanogr.*, 41, 451–459, 1996.

805 Planchon, F., Ballas, D., Cavagna, A.-J., Van Der Merwe, P., Bowie, A., Trull, T.,
806 Laurenceau, E., Davis, D., and Dehairs, F.: Carbon export in the naturally iron-
807 fertilized Kerguelen area of the Southern Ocean using ^{234}Th -based approach,
808 *Biogeosciences Discuss.*, doi:10.5194/bgd-11-15991-2014, 2014.

809 Rafter, P. A., DiFiore, P. J., and Sigman, D. M.: Coupled nitrate nitrogen and oxygen
810 isotopes and organic matter remineralization in the Southern and Pacific Oceans, *J.*
811 *Geophys. Res.–Oceans*, 118, 4781–4794, doi:10.1002/jgrc.20316, 2013.

812 Sigman, D. M., Altabet, M. A., McCorkle, D. C., Francois, R., and Fischer, G.: The $\delta^{15}\text{N}$ of
813 nitrate in the Southern Ocean: Consumption of nitrate in surface waters, *Global*
814 *Biogeochem. Cy.*, 13, 1149–1166, 1999.

815 Sigman, D. M., Altabet, M. A., McCorkle, D. C., Francois, R., and Fischer, G.: The $\delta^{15}\text{N}$ of
816 nitrate in the Southern Ocean: Nitrogen cycling and circulation in the ocean
817 interior, *J. Geophys. Res.-Oceans*, 105, 19,599–19,614, 2000.

818 Sigman, D. M., Casciotti, K. L., Andreani, M., Barford, C., Galanter, M., and Böhlke, J. K.:
819 A bacterial method for nitrogen isotopic analysis of nitrate in seawater and
820 freshwater, *Anal. Chem.*, 73, 4145–4153, 2001.

821 Sigman, D., Granger, J., DiFiore, P., Lehmann, M. M., Ho, R., Cane, G., and van Geen, A.:
822 Coupled nitrogen and oxygen isotope measurements of nitrate along the eastern
823 North Pacific margin, *Global Biogeochem. Cy.*, 19, GB4022,
824 doi:10.1029/2005GB002458, 2005.

825 Sigman, D. M., Karsh, K. L., and Casciotti, K. L.: Nitrogen isotopes in the ocean, in:
826 Encyclopedia of Ocean Sciences, edited by: Steele, J. H., Turekian, K. K., and
827 Thorpe, S. A., Elsevier, 25, 40–54, 2009a.

828 Sigman, D. M., DiFiore, P. J., Hain, M. P., Deutsch, C., Wang, Y., Karl, D. M., Knapp, A.
829 N., Lehmann, M. F., and Pantoja, S.: The dual isotopes of deep nitrate as a
830 constraint on the cycle and budget of oceanic fixed nitrogen, *Deep-Sea Res. Pt. I*,
831 56, 1419–1439, 2009b.

832 Stahl, D. A. and de la Torre, J.: Physiology and diversity of ammonia-oxidizing archaea,
833 *Annu. Rev. Microbiol.*, 66, 88–101, 2012.

834 Trull, T. W., Davies, D., and Casciotti, K.: Insights into nutrient assimilation and export
835 in naturally iron-fertilized waters of the Southern Ocean from nitrogen, carbon and
836 oxygen isotopes, *Deep-Sea Res. Pt. II*, 55, 820–84, 2008.

837 Trull, T.W., Davies, D., Dehairs, F., Cavagna, A.-J., Lasbleiz, M., Laurenceau, E.C.,
838 d'Ovidio, F., Planchon, F., Leblanc, K., Quéguiner, B., and Blain, S.: Chemometric
839 perspectives on plankton community responses to natural iron fertilization over
840 and downstream of the Kerguelen plateau in the Southern Ocean, *Biogeosciences*
841 *Discuss.*, doi:10.5194/bgd-11-13841-2014, 2014.

842 Wankel, S. D., Kendall, C., Pennington, J. T., Chavez, F. P., and Paytan, A.: Nitrification
843 in the euphotic zone as evidence by nitrate dual isotopic composition;
844 Observations from Monterey Bay, California, *Global Biogeochem. Cy.*, 21, GB2009,
845 doi:10.1029/2006GB002723, 2007.

846 Waser, N. A. D., Harrison, P. J., Nielsen, B., Calvert, S. E., and Turpin, D. H.: Nitrogen
847 isotope fractionation during the uptake and assimilation of nitrate, nitrite,
848 ammonium and urea by a marine diatom, *Limnol. Oceanogr.*, 43, 215–224, 1998.

849 Waser, N. A., Yu, Z., Yin, K., Nielsen, B., Harrison, P. J., Turpin, D. H., and Calvert, S. E.:
850 Nitrogen isotopic fractionation during a simulated diatom spring bloom:
851 importance of N- 15 starvation in controlling fractionation, *Mar. Ecol.-Prog. Ser.*,
852 179, 291–296, 1999.

853 Yool, A., Martin, A.P., Fernández, C., and Clark, D.R.: The significance of nitrification for
854 oceanic new production, *Nature*, 447, 999-1002, 2007.

855

856

857 Table headings:

858

859 Table 1: Average values for Sal, Tpot, Chl-a, NO_2^- , NH_4^+ , NO_3^- , Si(OH)_4 , $\delta^{15}\text{N}_{\text{NO}_3}$,
860 $\delta^{18}\text{O}_{\text{NO}_3}$ in the upper 100m, for the Plateau, Polar Front Meander, Polar Front sites
861 and the HNLC Reference station. Nutrient data are from the shipboard nutrient
862 team (Blain et al., 2014); Chl-a data are from Lasbleiz et al. (2014); ML depth values
863 are from Y.-H. Park pers. communic. .

864

865 Table 2: Considered isotopic discrimination factors for model calculations.

866

867 Table 3: Plateau and Meander sites: Observed initial and final conditions of nitrate
868 concentrations isotopic compositions; Observed nitrate and ammonium uptake
869 rates (from Cavagna et al., 2014); Calculated nitrification, nitrite uptake, nitrate
870 upwelling rates required to explain the observed nitrate isotopic compositions and
871 nitrate concentrations at the end of the considered growth period.

872

873 Appendix Table A1: Complete data set. Salinity; Tpot; density; $\delta^{15}\text{N}_{\text{NO}_3}$; $\delta^{18}\text{O}_{\text{NO}_3}$;
874 concentrations of NO_3^- ; NO_2^- ; NH_4^+ . Nutrient data are from Blain et al. (2014).

875

876

877 Figure legends:

878

879 Figure 1: (a) Kerguelen area with KEOPS 2 sampling grid. Blue dots = 'Plateau' stations;
880 Red dots = 'Meander' stations; Green dots = stations at the Polar Front and north
881 of the PF; black dot = 'Reference' station; Orange dots = stations outside the
882 Plateau and Meander areas. The black line marks the position of the Polar Front;
883 (b) MODIS Chlorophyll distribution for second half of November 2011 (colour bar:
884 $\mu\text{g l}^{-1}$); arrows represent the current speed, with scale marked by the small black
885 arrow (30cm/sec) below the figure (courtesy F. d'Ovidio & Y.-H. Park); (c) T-S
886 diagram (all stations) with $[\text{NO}_3^-]$ superimposed. (ODV-AWI, R. Schlitzer).

887 Figure 2: Water column profiles of (a) NO_3^- (μM); (b) $\delta^{15}\text{N}_{\text{NO}_3}$; (c) $\delta^{18}\text{O}_{\text{NO}_3}$, and (d) $\Delta(15-$
888 18); Complete data set. Blue circles = Plateau stations; Red circles = Meander
889 stations; Green circles = Polar Front and north of PF stations; Filled black circle =
890 Reference station (R-2).

891 Figure 3: Whole water column distributions of $\delta^{15}\text{N}_{\text{NO}_3}$, $\delta^{18}\text{O}_{\text{NO}_3}$, NO_3^- , Tpot and Salinity;
892 (a) West to east section starting on the Kerguelen Plateau and crossing the Polar
893 Front Meander; the Polar Front loop is crossed at about 71.3°E and at 74°E ; (b)
894 South to North section along about 72°E . (ODV-AWI, R. Schlitzer)

895 Figure 4: Regressions of $\delta^{15}\text{N}$ (left) and $\delta^{18}\text{O}$ (right) vs. $\text{LN}[\text{NO}_3^-]$; Top row: whole water
896 column; bottom row: upper 250m, Blue circles: Plateau stations; Red circles:
897 Meander stations; Green circles: Polar Front and north of Polar Front stations.

898 Figure 5: Profiles of $\delta^{18}\text{O}_{\text{NO}_3}$ and Chl-a ($\mu\text{g l}^{-1}$) profile for stations underlying the high
899 Chlorophyll plume in the vicinity of the Polar Front (green circles; stations TEW7,
900 TEW8, F-L) and in the central part of the Polar Front Meander (red circles; stations
901 TNS6, TNS1, TEW6) and the Reference station (black circles; station R-2).

902 Figure 6: Sections of NH_4^+ , NO_2^- , $\delta^{15}\text{N}_{\text{NO}_3}$, $\delta^{18}\text{O}_{\text{NO}_3}$ and $\Delta(15-18)$ in the upper 600m of
903 water column; (a) West to East section; (b) South to north section. NH_4^+ and NO_2^-
904 data are from Blain et al. (2014). (ODV-AWI, R. Schlitzer).

905 Figure 7: Profiles of NH_4^+ (μM) and NO_2^- (μM) in the upper 500m for Plateau (blue
906 circles); Meander (red circles); Polar Front (green circles). Superimposed are the

907 late season data for the Plateau region as recorded during KEOPS 1 (Trull et al.,
908 2008).

909 Figure 8: $\delta^{18}\text{O}_{\text{NO}_3}$ vs. $\delta^{15}\text{N}_{\text{NO}_3}$; Blue = Plateau; Red = Meander; Green = Polar Front and
910 north of PF; (a) whole water column; (b) Upper 250 m; (c) Mixed Layer; Grey circles
911 in (B) and (C) represent the late season Plateau values recorded during KEOPS 1
912 (Trull et al., 2008); the black line with slope = 1 represents the evolution of
913 reference deep water nitrate with $\delta^{15}\text{N}_{\text{NO}_3} = 5\text{‰}$ and $\delta^{18}\text{O}_{\text{NO}_3} = 2\text{‰}$ in case the
914 $^{15}\text{N}/^{14}\text{N}$ and $^{18}\text{O}/^{16}\text{O}$ fractionation factors are similar.

915

916 Table 1: Average values for Sal, Tpot, Chl-a, NO₃⁻, NO₂⁻, NH₄⁺, Si(OH)₄, δ¹⁵N_{NO3}, δ¹⁸O_{NO3} in the upper 100m, for the Plateau, Polar Front Meander, Polar Front sites and the
 917 HNLC Reference station. Nutrient data are from the shipboard nutrient team (Blain et al., 2014); Chl-a data are from Lasbleiz et al. (2014); ML depth values are from Y.-H.
 918 Park, pers. communic. .

919

Region	Station	CTD	Julian Day	Long. °E	Lat. °S	MLD m	Sal		Tpot °C		Chl-a µg L ⁻¹		[NO ₃], µM		[NO ₂], µM		[NH ₄ ⁺], µM		[Si(OH) ₄] µM		δ ¹⁵ N _{NO3} ‰		δ ¹⁸ O _{NO3} ‰	
							ML	100m	ML	100m	ML	100m	ML	100m	ML	100m	ML	100m	ML	100m	ML	100m	ML	100m
<i>Reference</i>	R-2	17	298	66.69	-50.39	111	33.774	33.773	2.073	2.125	0.249	0.29	25.72	25.7	0.32	0.32	0.320	0.32	12.34	12.20	6.16	6.16	4.12	4.12
<i>Plateau</i>	A3-1	4	293	72.08	-50.63	160	33.905	33.900	1.715	1.706	0.70	0.70	29.5	29.3	0.27	0.27	0.12	0.10	23.74	23.35	5.82	5.85	3.38	3.40
	TNS8	8	295	72.24	-49.46	139	33.871	33.869	2.066	2.108	0.75	0.78	28.6	28.4	0.27	0.28	0.20	0.19	17.59	17.19	6.12	6.11	3.67	3.57
	TEW4	42	305	71.62	-48.63	95	33.858	33.858	2.517	2.517	1.20	1.20	25.9	25.9	0.26	0.26	0.20	0.20	14.40	14.40	6.11	6.11	3.90	3.90
	E4W1	81	315	71.43	-48.77	67	33.899	33.903	2.605	2.417	1.39	1.07	24.8	25.6	0.28	0.29	0.10	0.12	17.46	18.96	6.49	6.30	3.58	3.43
	E4W2	111	322	71.43	-48.77	35	33.859	33.873	2.910	2.641	1.80	1.88	23.2	24.3	0.27	0.27	0.12	0.39	8.72	11.28	7.02	6.94	5.16	5.03
	A3-2	99	320	72.06	-50.62	143	33.914	33.913	2.194	2.219	2.03	1.97	25.8	25.8	0.33	0.33	0.20	0.20	18.96	18.72	6.37	6.42	4.38	4.46
	<i>average</i>							<i>33.884</i>	<i>33.886</i>	<i>2.334</i>	<i>2.268</i>	<i>1.31</i>	<i>1.27</i>	<i>26.3</i>	<i>26.6</i>	<i>0.28</i>	<i>0.28</i>	<i>0.16</i>	<i>0.20</i>	<i>16.81</i>	<i>17.31</i>	<i>6.32</i>	<i>6.29</i>	<i>4.01</i>
<i>± 1sd</i>							<i>0.024</i>	<i>0.022</i>	<i>0.427</i>	<i>0.337</i>	<i>0.54</i>	<i>0.54</i>	<i>2.4</i>	<i>1.9</i>	<i>0.03</i>	<i>0.03</i>	<i>0.05</i>	<i>0.10</i>	<i>5.00</i>	<i>4.15</i>	<i>0.41</i>	<i>0.37</i>	<i>0.66</i>	<i>0.65</i>

920

921

922

923 Table 1: Continued

924

Region	Station	CTD	Julian Day	Long. °E	Lat. °S	MLD m	Sal		Tpot °C		Chl-a µg L ⁻¹		[NO ₃], µM		[NO ₂], µM		[NH ₄ ⁺], µM		[Si(OH) ₄] µM		δ ¹⁵ N _{NO3} ‰		δ ¹⁸ O _{NO3} ‰	
							ML	100m	ML	100m	ML	100m	ML	100m	ML	100m	ML	100m	ML	100m	ML	100m	ML	100m
<i>Meander</i>	TNS6	10	295	72.28	-48.78	67	33.847	33.849	2.311	2.246	0.70	0.68	27.3	27.4	0.28	0.29	0.35	0.38	16.53	16.74	6.08	6.08	3.66	3.68
	E1	27	302	72.19	-48.46	83	33.854	33.857	2.479	2.415	0.94	0.90	25.5	25.4	0.26	0.27	0.23	0.27	15.14	15.46	6.25	6.24	4.02	4.00
	TEW5	44	306	72.80	-48.47	61	33.850	33.853	2.501	2.371	0.86	0.72	26.5	27.0	0.27	0.28	0.30	0.34	14.98	15.71	6.25	6.18	3.71	3.72
	TEW6	45	306	73.40	-48.47	56	33.845	33.848	2.642	2.530	0.80	0.70	26.4	26.8	0.26	0.27	0.33	0.36	15.71	16.17	6.17	6.10	4.12	3.96
	E3	50	307	71.97	-48.70	51	33.846	33.851	2.726	2.507	0.63	0.49	25.6	26.5	0.27	0.28	0.30	0.37	15.10	16.30	6.17	6.08	3.37	3.52
	E4E	94	317	72.56	-48.72	77	33.834	33.854	3.192	2.631	1.11	0.73	24.4	25.6	0.26	0.26	0.22	0.37	12.23	15.10	6.64	6.30	4.04	3.53
	E5	114	322	71.90	-48.41	35	33.842	33.849	3.174	3.022	1.15	1.07	25.2	25.6	0.25	0.26	0.36	0.45	11.71	12.39	6.57	6.52	3.95	4.26
	IODA REC <i>average</i> <i>± 1sd</i>	120	324	72.89	-48.36	50	33.822	33.830	3.438	3.169	1.82	1.51	23.9	24.9	0.27	0.22	0.43	0.51	10.50	12.25	6.88	6.63	5.16	5.16
						<i>33.842</i>	<i>33.849</i>	<i>2.808</i>	<i>2.611</i>	<i>1.00</i>	<i>0.85</i>	<i>25.6</i>	<i>26.2</i>	<i>0.27</i>	<i>0.26</i>	<i>0.32</i>	<i>0.38</i>	<i>13.99</i>	<i>15.02</i>	<i>6.38</i>	<i>6.27</i>	<i>4.00</i>	<i>3.98</i>	
						<i>0.010</i>	<i>0.008</i>	<i>0.407</i>	<i>0.322</i>	<i>0.38</i>	<i>0.32</i>	<i>1.1</i>	<i>0.9</i>	<i>0.01</i>	<i>0.02</i>	<i>0.07</i>	<i>0.07</i>	<i>2.19</i>	<i>1.74</i>	<i>0.28</i>	<i>0.21</i>	<i>0.53</i>	<i>0.54</i>	
<i>Polar Front</i>	TEW7	46	306	74.00	-48.47	47	33.785	33.805	3.994	3.533	3.24	2.07	20.2	23.2	0.25	0.24	0.24	0.33	6.78	10.62	7.28	6.67	4.69	4.11
	TEW8	47	307	75.00	-48.47	24	33.777	33.802	3.899	3.236	2.85	1.59	21.2	24.3	0.24	0.24	0.29	0.36	8.23	12.59	6.74	6.35	4.73	4.17
	F-L	63	310	74.66	-48.53	40	33.748	33.772	4.180	3.711	4.00	2.43	19.6	21.7	0.27	0.28	0.24	0.30	7.34	10.57	7.51	6.86	5.24	4.37
	<i>average</i>						<i>33.770</i>	<i>33.793</i>	<i>3.023</i>	<i>3.493</i>	<i>2.58</i>	<i>2.03</i>	<i>20.3</i>	<i>23.1</i>	<i>0.25</i>	<i>0.25</i>	<i>0.20</i>	<i>0.33</i>	<i>5.91</i>	<i>11.26</i>	<i>7.18</i>	<i>6.63</i>	<i>3.73</i>	<i>4.22</i>
	<i>± 1sd</i>						<i>0.019</i>	<i>0.015</i>	<i>2.006</i>	<i>0.196</i>	<i>1.63</i>	<i>0.42</i>	<i>0.8</i>	<i>1.0</i>	<i>0.02</i>	<i>0.02</i>	<i>0.12</i>	<i>0.03</i>	<i>3.14</i>	<i>1.16</i>	<i>0.40</i>	<i>0.21</i>	<i>2.33</i>	<i>0.11</i>

925

926

927

928

929

930 Table 2: Considered isotopic discrimination factors for model calculations.

931

Parameter, Process	d ¹⁸ O, ‰	e ¹⁵ ; e ¹⁸ ‰	References
d ¹⁸ O-H ₂ O	-0.4		Archambeau et al., 1998
Remineralisation		0 - 2	Kendall, 1998; Knapp et al., 2011; Möbius, 2013
NO ₃ ⁻ uptake		4.5 - 6.3	Waser et al., 1998; Granger et al., 2010; DiFiore et al., 2010
NH ₄ ⁺ uptake		0 - 5*	Hoch et al., 1992; Fogel & Cifuentes, 1993; Pennock et al., 1996; Waser et al. 1999
NH ₄ ⁺ oxidation		15	Casciotti et al., 2003; DiFiore et al., 2009
NO ₂ ⁻ oxidation		-12 - -13	Casciotti, 2009; Buchwald and Casciotti, 2010
NO ₂ ⁻ Uptake		0 - 1	Waser et al., 1998

* for low ammonium concentrations (<10 µM)

932

933

934 Table 3: Plateau and Meander sites: Observed initial and final conditions of nitrate concentration and isotopic composition; Observed nitrate and ammonium uptake rates (from Cavagna et
 935 al., 2014); Calculated nitrification, nitrite uptake, nitrate upwelling rates required to explain the observed nitrate isotopic composition and nitrate concentration at the end of the
 936 considered growth period.

	[NO ₃ ⁻] μM	δ ¹⁵ N _{NO3} ‰	δ ¹⁸ O _{NO3} ‰	Measured Flux mmol m ⁻² d ⁻¹	Best fit (min. - max.) mmol m ⁻² d ⁻¹	Best fit (min. - max.); fixed upwelling ^c mmol m ⁻² d ⁻¹
Plateau						
Upwelling water	29.9	5.74	3.31			
Average condition in upper 100m (A3-1); T0	29.3	5.85	3.40			
Average condition in upper 100m (A3-2); Tend	25.8	6.42	4.46			
NO ₃ ⁻ uptake				36.5 ± 4.7 ^a		
NH ₄ ⁺ uptake				6.2 ± 1.9 ^a		
Calculated: Uptake only (Rayleigh)	19.4	7.92	5.47			
Calculated: Nitrification					17.4 ; (6 - 27)	16.2 ; (10 - 22)
Calculated: NO ₃ ⁻ upwelling					6.2 ; (0 - 24)	7.4
Calculated: NO ₂ ⁻ Uptake					6.1 ; (0 - 17)	5.6; (0 - 14)
Polar Front Meander						
Upwelling water	31.6	5.32	2.85			
Average condition in upper 100m (TNS6); T0	27.4	6.17	3.74			
Average condition in upper 100m (E5); Tend	25.6	6.62	4.33			
NO ₃ ⁻ uptake				12.4 ± 2.2 ^a		
NH ₄ ⁺ uptake				6.6 ± 1.4 ^a		
Calculated: Uptake only (Rayleigh)	24.0	6.73	4.33			
Calculated: Nitrification					1.7 ; (0 - 11)	1.3 ; (0 - 6)
Calculated: NO ₃ ⁻ upwelling					4.0 ; (0 - 11)	7.4
Calculated: NO ₂ ⁻ Uptake					0	0

^a average rates from Cavagna et al. (2014)

^b matching with observed value at T_{end} is imposed

^c Nitrate upwelling fixed at 7.4 mmol m⁻² d⁻¹, based on the Ekman pumping velocity in Gille et al. (2014)

937

Table A1: Complete data set. Salinity; Tpot; density; $\delta^{15}\text{N}_{\text{NO}_3}$; $\delta^{18}\text{O}_{\text{NO}_3}$; concentrations of NO_3^- ; NO_2^- ; NH_4^+ ; Nutrient data are from Blain et al. (2014).

Station Name	Lon °E	Lat °S	Seafloor, m	CTD N°	Depth, m	Salinity	Tpot °C	Density, σ_θ	$\delta^{15}\text{N}_{\text{NO}_3}$, ‰	$\delta^{18}\text{O}_{\text{NO}_3}$, ‰	$[\text{NO}_3^-]$, μM	$[\text{NO}_2^-]$, μM	$[\text{NH}_4^+]$, μM
A3-1	72.08	-50.63	530	4	469	34.359	2.184	27.443	5.28	3.08	35.4	0.05	0.05
					352	34.254	2.106	27.366	5.37	2.99	34.9	0.04	0.01
					278	34.137	1.821	27.294	5.61	3.71	33.7	0.03	0.03
					252	34.099	1.744	27.270	5.45	2.92	33.4	0.04	0.01
					227	34.062	1.769	27.238	5.65	3.37	32.9	0.04	-
					202	34.011	1.693	27.203	5.63	3.20	32.1	0.05	0.04
					173	33.934	1.670	27.142	5.79	-	30.7	0.2	0.06
					151	33.915	1.740	27.122	5.74	3.31	29.9	0.26	0.16
					101	33.904	1.727	27.114	5.85	3.55	29.7	0.26	0.12
					41	33.897	1.698	27.111	5.89	3.43	29.2	0.27	0.08
					12	33.896	1.695	27.110	5.80	3.22	28.8	0.27	0.11
TNS8	72.24	-49.46	1030	8	992	34.660	2.169	27.686	5.08	3.36	34.7	0.04	-
					903	34.642	2.201	27.669	5.00	2.64	34.7	0.03	-
					702	34.565	2.257	27.602	4.93	-	34.7	0.03	-
					601	34.528	2.283	27.571	5.09	2.11	36.2	0.03	-
					501	34.466	2.268	27.523	5.17	2.19	36.7	0.03	-
					401	34.374	2.182	27.456	5.27	2.41	36.2	0.03	0
					303	34.244	1.954	27.369	5.42	2.31	35.7	0.04	0
					251	34.113	1.909	27.268	5.40	2.50	34.2	0.04	0
					203	33.912	1.796	27.116	5.89	4.15	30.0	0.18	0.17
					149	33.877	1.903	27.079	6.10	3.81	29.5	0.26	0.26
					101	33.870	2.055	27.062	6.15	3.52	28.4	0.27	0.19
41	33.867	2.126	27.054	6.10	3.74	28.6	0.28	0.19					
12	33.867	2.126	27.054	6.07	3.41	28.1	0.28	0.20					

938

939

940 Table A1: Continued

Station Name	Lon °E	Lat °S	Seafloor, m	CTD N°	Depth, m	Salinity	Tpot °C	Density, σ_θ	$\delta^{15}\text{N}_{\text{NO}_3}$, ‰	$\delta^{18}\text{O}_{\text{NO}_3}$, ‰	$[\text{NO}_3^-]$, μM	$[\text{NO}_2^-]$, μM	$[\text{NH}_4^+]$, μM
TNS6	72.28	-48.78	1885	10	1871	34.742	1.621	27.794	4.87	2.56	31.3	0.01	-
					1514	34.740	1.835	27.776	4.92	2.32	31.7	0	-
					807	34.628	2.280	27.651	5.30	2.26	34.6	0.01	-
					605	34.522	2.290	27.565	4.87	2.38	35.1	0.01	-
					505	34.470	2.352	27.518	4.96	2.74	35.5	0.02	-
					404	34.345	2.102	27.439	5.14	1.95	35.9	0.01	0
					303	34.244	2.082	27.360	5.26	2.03	34.6	0.02	0.02
					253	34.116	1.940	27.268	5.16	2.46	33.2	0.02	0.01
					202	34.035	2.059	27.194	5.49	2.99	32.4	0.03	0.01
					183	33.995	2.012	27.165	5.32	2.85	31.6	0.04	0.01
					102	33.852	2.056	27.047	6.07	3.71	27.5	0.29	0.45
					41	33.845	2.296	27.023	6.01	3.72	27.5	0.28	0.38
					12	33.844	2.426	27.012	6.15	3.59	27.0	0.28	0.25
					TNS1	71.50	-46.83	2280	15	2263	34.743	1.330	27.816
1508	34.748	2.100	27.762	5.21						2.18	29.9	0.04	0
802	34.547	2.435	27.573	5.12						2.08	33.7	0.03	0
602	34.431	2.542	27.472	5.25						2.96	33.5	0.05	0
502	34.308	2.539	27.373	5.41						3.44	-	-	-
402	34.209	2.492	27.298	5.49						4.55	34.1	0.03	0
302	34.061	2.446	27.184	5.75						4.01	30.8	0.03	0
251	33.990	2.579	27.116	5.75						3.93	29.1	0.07	0
201	33.891	2.819	27.015	6.23						3.94	27.4	0.04	0
151	33.780	3.020	26.910	6.23						5.16	25.9	0.11	0
102	33.718	3.784	26.788	6.27						4.70	24.1	0.31	0.19
41	33.714	3.994	26.764	6.82						5.09	23.7	0.29	0.11
11	33.714	4.168	26.746	6.63						5.26	23.9	0.3	0.08

941

942

943 Table A1: Continued

Station Name	Lon °E	Lat °S	Seafloor, m	CTD N°	Depth, m	Salinity	Tpot °C	Density, σ_θ	$\delta^{15}\text{N}_{\text{NO}_3}$, ‰	$\delta^{18}\text{O}_{\text{NO}_3}$, ‰	[NO ₃], μM	[NO ₂], μM	[NH ₄ ⁺], μM
R-2	66.72	-50.36	2532	17	904	34.616	2.329	27.637	5.16	2.52	33.9	0.03	-
					703	34.516	2.369	27.554	5.09	2.04	35.2	0.04	-
					603	34.440	2.413	27.489	5.17	2.23	35.3	0.07	-
					503	34.343	2.306	27.421	5.04	2.51	35.1	0.04	-
					401	34.250	2.263	27.350	5.19	2.61	34.1	0.04	-
					251	34.018	2.028	27.183	5.53	2.91	-	-	-
					201	33.900	1.860	27.101	5.37	3.14	28.8	0.05	-
					100	33.771	2.025	26.985	6.12	-	25.8	0.32	-
					79	33.770	2.104	26.978	6.12	4.03	25.9	0.32	-
					40	33.771	2.174	26.973	6.24	3.91	25.7	0.32	-
					21	33.771	2.177	26.973	6.14	3.82	25.4	0.31	-
R-2	66.69	-50.39	2450	20	2453	34.734	1.107	27.824	4.81	1.96	32.8	0.04	-
					1817	34.759	1.686	27.803	5.07	2.12	31.5	0.04	-
					1508	34.750	1.953	27.775	4.96	1.75	31.5	0.05	-
					1003	34.663	2.288	27.678	5.15	2.12	33.6	0.04	-
					806	34.584	2.346	27.610	5.12	2.37	35.6	0.03	-
					605	34.455	2.410	27.502	5.13	2.39	36.9	0.04	-
					503	34.367	2.428	27.429	5.13	2.02	36.8	0.03	-
					353	34.180	2.251	27.295	5.43	2.32	34.5	0.04	-

944

945

946

947 Table A1: Continued

Station Name	Lon °E	Lat °S	Seafloor, m	CTD N°	Depth, m	Salinity	Tpot °C	Density, σ_θ	$\delta^{15}\text{N}_{\text{NO}_3}$, ‰	$\delta^{18}\text{O}_{\text{NO}_3}$, ‰	[NO ₃], μM	[NO ₂], μM	[NH ₄ ⁺], μM
E1	72.19	-48.46	2056	27	906	34.644	2.202	27.670	5.17	2.49	33.2	0.02	-
					702	34.569	2.231	27.608	5.17	2.59	33.8	0.02	-
					600	34.520	2.235	27.568	5.15	2.30	34.0	0.03	-
					501	34.465	2.251	27.523	5.23	2.51	35.1	0.03	-
					400	34.385	2.188	27.464	5.32	2.68	34.5	0.03	-
					301	34.236	1.962	27.362	5.25	2.73	-	-	-
					251	34.148	1.870	27.299	5.24	2.66	-	-	-
					180	33.964	1.813	27.156	5.71	3.46	29.3	0.08	0.01
					150	33.881	2.012	27.074	5.97	3.71	27.3	0.26	0.30
					124	33.874	2.139	27.059	6.32	4.41	26.4	0.27	0.41
					100	33.865	2.212	27.046	6.20	3.95	25.4	0.27	0.39
					81	33.855	2.375	27.025	6.04	3.85	25.9	0.27	0.32
					40	33.852	2.500	27.012	6.25	3.87	25.5	0.26	0.19
E1	72.18	-48.50	2058	30	2025	34.740	1.416	27.808	4.94	1.98	33.0	0.03	-
					1486	34.737	1.860	27.772	4.93	2.41	32.2	0.03	-
					1003	34.675	2.179	27.697	5.00	2.90	34.2	0.03	-
					802	34.623	2.263	27.649	5.15	2.85	35.6	0.03	-
					631	34.554	2.270	27.592	5.22	2.69	36.9	0.03	-
					501	34.477	2.321	27.527	5.18	1.99	36.7	0.04	-
					451	34.434	2.306	27.493	5.23	2.35	37.0	0.04	-
					350	34.326	2.171	27.418	5.06	2.25	36.2	0.04	-
300	34.249	1.972	27.372	5.06	2.46	35.5	0.04	-					

948

949

950

951 Table A1: Continued

Station Name	Lon °E	Lat °S	Seafloor, m	CTD N°	Depth, m	Salinity	Tpot °C	Density, σ_θ	$\delta^{15}\text{N}_{\text{NO}_3}$, ‰	$\delta^{18}\text{O}_{\text{NO}_3}$, ‰	[NO ₃], μM	[NO ₂], μM	[NH ₄ ⁺], μM
TEW1	69.83	-49.15	92	35	71	33.656	2.519	26.854	6.08	3.95	27.1	0.34	1.15
					60	33.652	2.575	26.846	5.93	3.59	26.9	0.33	0.99
					51	33.639	2.722	26.823	6.20	4.03	26.2	0.31	1.02
					41	33.627	2.830	26.804	6.19	3.86	25.5	0.31	0.78
					31	33.621	2.922	26.791	6.34	4.00	25.6	0.31	0.67
					20	33.620	2.981	26.786	6.40	4.18	24.4	0.31	0.52
					10	33.611	3.369	26.743	6.70	4.40	23.6	0.31	0.19
TEW3	71.02	-48.80	570	38	541	34.369	2.184	27.452	4.85	2.43	34.0	0.04	0.01
					401	34.253	2.148	27.361	5.04	2.44	33.9	0.07	0
					276	34.107	2.073	27.251	5.07	2.72	31.6	0.07	0
					252	34.095	2.064	27.242	5.34	2.53	31.6	0.07	0
					182	33.953	1.974	27.134	5.46	3.16	28.4	0.19	0.08
					111	33.892	1.980	27.085	5.57	3.39	27.8	0.27	0.18
					91	33.879	2.025	27.072	5.73	3.97	27.9	0.24	0.15
					76	33.876	2.075	27.065	5.92	3.79	27.1	0.24	0.13
					61	33.872	2.131	27.058	6.18	3.66	27.2	0.24	0.09
					40	33.865	2.137	27.052	6.04	3.78	27.2	0.25	0.12
16	33.868	2.315	27.040	5.91	3.73	26.5	0.25	0.09					

952

953

954

Station Name	Lon °E	Lat °S	Seafloor, m	CTD N°	Depth, m	Salinity	Tpot °C	Density, σ_θ	$\delta^{15}\text{N}_{\text{NO}_3}$, ‰	$\delta^{18}\text{O}_{\text{NO}_3}$, ‰	[NO ₃], μM	[NO ₂], μM	[NH ₄ ⁺], μM
TEW4	71.62	-48.63	1579	42	1567	34.730	1.895	27.764	5.16	2.08	31.7	0.03	-
					1004	34.662	2.164	27.688	4.88	2.02	33.6	0.03	-
					802	34.598	2.242	27.630	4.91	2.34	34.5	0.03	-
					602	34.514	2.275	27.560	4.94	1.81	35.2	0.03	-
					502	34.438	2.238	27.502	4.97	2.01	35.5	0.03	-
					301	34.193	1.887	27.334	5.08	2.05	-	-	-
					300	34.189	1.882	27.331	5.13	2.26	33.9	0.03	0
					251	34.086	1.773	27.256	4.93	2.00	33.1	0.03	0
					201	33.928	1.733	27.133	5.52	2.82	29.8	0.19	0.16
					151	33.892	1.903	27.091	5.80	3.62	28.1	0.25	0.36
					101	33.865	2.370	27.033	5.95	3.37	26.1	0.26	0.37
					41	33.854	2.567	27.008	6.17	4.04	25.5	0.25	0.13
					11	33.855	2.618	27.004	6.20	4.30	25.3	0.25	0.11
					TEW5	72.80	-48.47	2275	44	2271	34.730	1.130	27.820
1003	34.685	2.181	27.705	5.04						1.63	33.9	0.03	-
801	34.621	2.252	27.647	5.06						2.25	34.7	0.04	-
601	34.522	2.277	27.566	4.86						1.65	36.4	0.04	-
501	34.446	2.240	27.509	5.11						2.50	35.7	0.04	-
401	34.351	2.140	27.440	5.15						2.23	35.1	0.04	0
301	34.210	1.997	27.339	5.23						2.12	34.6	0.05	0
251	34.106	1.890	27.264	5.27						3.11	32.6	0.04	0
201	33.959	1.833	27.150	5.50						2.81	30.8	0.08	0.01
151	33.880	1.840	27.087	5.70						3.42	28.9	0.26	0.30
101	33.858	2.016	27.055	5.97						3.73	28.5	0.3	0.48
60	33.851	2.376	27.021	6.24						3.57	26.3	0.29	0.43
41	33.849	2.508	27.008	6.10						3.57	26.6	0.27	0.27
10	33.848	2.704	26.992	6.43						4.00	26.6	0.26	0.19

Station Name	Lon °E	Lat °S	Seafloor, m	CTD N°	Depth, m	Salinity	Tpot °C	Density, σ_θ	$\delta^{15}\text{N}_{\text{NO}_3}$, ‰	$\delta^{18}\text{O}_{\text{NO}_3}$, ‰	$[\text{NO}_3^-]$, μM	$[\text{NO}_2^-]$, μM	$[\text{NH}_4^+]$, μM
TEW6	73.40	-48.47	2410	45	2403	34.710	0.709	27.831	4.73	2.08	33.3	0.03	-
					1004	34.675	2.204	27.695	5.16	2.22	33.7	0.03	-
					802	34.621	2.257	27.647	4.75	1.89	34.6	0.03	-
					602	34.544	2.283	27.584	4.95	2.53	35.1	0.03	-
					502	34.471	2.232	27.529	5.02	1.84	35.5	0.03	-
					401	34.392	2.170	27.471	5.07	2.37	35.5	0.03	0
					302	34.256	2.056	27.371	5.12	2.76	35.1	0.03	0
					251	34.164	2.080	27.296	5.22	2.07	34.5	0.03	0
					202	34.057	1.952	27.220	5.22	2.57	32.8	0.04	0.01
					151	33.919	1.783	27.122	5.82	3.31	30.5	0.08	0.01
					101	33.855	2.198	27.039	5.89	3.48	28.0	0.29	0.46
					61	33.844	2.499	27.006	6.08	3.50	27.0	0.27	0.49
					41	33.842	2.569	26.998	6.10	3.61	26.5	0.25	0.29
					12	33.844	2.959	26.966	6.28	5.28	25.6	0.25	0.22
TEW7	74.00	-48.47	2510	46	2503	34.700	0.497	27.836	4.59	1.67	33.2	0.03	-
					1506	34.734	1.975	27.760	4.82	1.89	31.7	0.02	-
					802	34.580	2.320	27.609	4.86	1.41	34.4	0.02	-
					601	34.483	2.386	27.526	5.15	1.72	35.1	0.02	-
					501	34.380	2.331	27.448	5.01	1.97	36.0	0.02	-
					401	34.253	2.541	27.329	5.26	2.10	35.3	0.02	0
					301	34.194	3.018	27.240	5.57	2.46	32.7	0.02	0
					251	34.157	3.264	27.188	5.48	2.59	32.7	0.03	0
					201	34.098	3.440	27.124	5.63	2.80	30.7	0.03	0
					150	34.009	3.308	27.066	5.65	3.18	30.0	0.07	0.01
					101	33.849	2.709	26.992	5.77	3.03	27.7	0.21	0.37
					61	33.794	3.446	26.881	6.34	4.02	24.8	0.24	0.47
41	33.788	3.825	26.839	7.04	4.40	21.6	0.24	0.38					
10	33.781	4.226	26.793	7.52	4.97	18.9	0.25	0.10					

Station Name	Lon °E	Lat °S	Seafloor, m	CTD N°	Depth, m	Salinity	Tpot °C	Density, σ_θ	$\delta^{15}\text{N}_{\text{NO}_3}$, ‰	$\delta^{18}\text{O}_{\text{NO}_3}$, ‰	$[\text{NO}_3^-]$, μM	$[\text{NO}_2^-]$, μM	$[\text{NH}_4^+]$, μM
TEW8	75.00	-48.47	2786	47	2788	34.695	0.399	27.838	4.27	1.58	33.0	0.02	-
					1003	34.665	2.348	27.675	4.48	1.31	33.3	0.02	-
					803	34.593	2.395	27.613	4.63	1.50	34.5	0.02	-
					604	34.449	2.394	27.498	4.54	1.47	35.1	0.02	-
					503	34.362	2.304	27.436	4.56	1.87	35.5	0.02	-
					403	34.273	2.280	27.367	4.74	1.72	35.5	0.03	0
					301	34.077	1.970	27.234	5.16	2.76	32.7	0.02	0
					252	34.024	2.147	27.178	4.77	1.97	32.0	0.03	0
					201	33.946	2.048	27.123	5.24	3.02	30.4	0.05	0
					151	33.881	2.107	27.067	5.65	2.90	29.2	0.26	0.11
					101	33.844	2.280	27.024	5.57	3.06	27.7	0.25	0.43
					40	33.785	3.596	26.860	5.49	3.18	-	-	-
					40	33.786	3.621	26.858	6.28	4.17	23.4	0.23	0.45
					11	33.766	4.197	26.785	7.19	5.29	18.9	0.25	0.12
					E3	71.97	-48.70	1915	50	904	34.645	2.233	27.668
701	34.570	2.300	27.603	4.84						1.68	35.5	0.03	-
603	34.515	2.272	27.561	4.74						1.46	36.2	0.03	-
500	34.462	2.255	27.520	5.00						1.79	-	-	-
402	34.346	2.146	27.436	4.91						1.43	36.1	0.03	0
201	33.932	1.765	27.134	5.38						2.89	31.1	0.1	0.01
153	33.883	1.940	27.081	5.91						3.04	27.9	0.29	0.39
124	33.886	2.107	27.071	5.92						2.89	27.7	0.27	0.53
101	33.861	2.082	27.053	5.80						3.81	28.2	0.3	0.45
71	33.853	2.261	27.032	6.05						3.65	27.5	0.3	0.51
41	33.846	2.687	26.991	6.08	3.30	26.5	0.27	0.30					
11	33.845	2.908	26.971	6.24	3.43	25.4	0.27	0.24					

960

961

962 Table A1: Continued

Station Name	Lon °E	Lat °S	Seafloor, m	CTD N°	Depth, m	Salinity	Tpot °C	Density, σ_θ	$\delta^{15}\text{N}_{\text{NO}_3}$, ‰	$\delta^{18}\text{O}_{\text{NO}_3}$, ‰	[NO ₃], μM	[NO ₂], μM	[NH ₄ ⁺], μM					
E3	71.97	-48.70	1910	55	1893	34.743	1.641	27.794	4.78	1.65	30.6	0.02	-					
					1204	34.703	2.107	27.725	4.72	1.23	31.6	0.02	-					
					1004	34.663	2.174	27.688	4.63	0.96	33.1	0.02	-					
					903	34.639	2.202	27.666	4.52	0.97	32.9	0.02	-					
					803	34.613	2.220	27.644	4.82	1.01	33.9	0.02	-					
					601	34.536	2.287	27.577	4.81	1.50	34.2	0.02	-					
					501	34.458	2.264	27.516	4.83	1.22	34.1	0.02	-					
					451	34.398	2.208	27.472	4.84	1.55	34.1	0.02	-					
					401	34.340	2.132	27.433	4.94	1.69	33.3	0.02	-					
					225	34.068	1.890	27.233	5.14	2.65	32.0	0.03	-					
					106	33.851	2.189	27.037	5.88	3.09	26.6	0.3	-					
					51	33.846	2.556	27.002	6.20	3.38	25.1	0.26	-					
					F-L	74.66	-48.53	2695	63	903	34.607	2.356	27.628	4.96	1.39	34.3	0.02	-
										502	34.388	2.674	27.426	5.13	1.97	35.3	0.02	-
401	34.355	3.050	27.366	5.26						2.02	35.2	0.03	-					
302	34.206	2.879	27.262	5.33						1.80	33.8	0.03	0					
151	33.905	2.250	27.075	5.46						3.54	29.9	0.04	0					
126	33.878	2.354	27.045	5.58						3.34	29.4	0.14	0					
101	33.836	2.631	26.988	5.82						2.97	28.4	0.31	0.19					
82	33.794	3.176	26.907	6.00						3.46	26.8	0.27	0.43					
61	33.749	3.917	26.799	6.81						4.12	22.9	0.27	0.45					
35	33.747	4.030	26.787	7.10						4.69	21.5	0.27	0.30					
11	33.744	4.318	26.754	7.74	5.44	18.9	0.27	0.08										

963

964

965

Station Name	Lon °E	Lat °S	Seafloor, m	CTD N°	Depth, m	Salinity	Tpot °C	Density, σ_θ	$\delta^{15}\text{N}_{\text{NO}_3}$, ‰	$\delta^{18}\text{O}_{\text{NO}_3}$, ‰	$[\text{NO}_3^-]$, μM	$[\text{NO}_2^-]$, μM	$[\text{NH}_4^+]$, μM					
F-L	74.81	-48.62	2739	68	2719	34.691	0.322	27.839	4.73	2.09	31.5	0.03	-					
					1758	34.746	1.758	27.787	4.87	1.28	32.4	0.03	-					
					1205	34.706	2.266	27.715	4.81	1.56	34.0	0.03	-					
					1005	34.657	2.388	27.665	4.97	1.57	34.0	0.03	-					
					902	34.620	2.443	27.631	4.91	1.42	36.2	0.03	-					
					602	34.471	2.731	27.487	5.13	1.12	36.3	0.04	-					
					502	34.391	2.677	27.427	5.16	1.33	36.4	0.03	-					
					452	34.356	2.643	27.403	5.08	1.84	35.9	0.03	-					
					402	34.316	2.769	27.360	5.09	1.93	35.2	0.03	-					
					302	34.257	3.185	27.275	5.28	1.91	34.0	0.04	-					
					30	33.749	4.194	26.771	7.70	5.58	18.6	0.28	-					
					E4W1	71.43	-48.77	1400	81	903	34.601	2.223	27.634	4.94	1.86	35.1	0.02	-
										703	34.539	2.219	27.585	4.88	1.50	35.1	0.02	-
603	34.507	2.250	27.557	4.84						1.33	35.8	0.02	-					
503	34.457	2.196	27.521	4.79						1.85	35.5	0.02	-					
402	34.368	2.130	27.455	4.99						1.62	35.6	0.02	0.01					
202	34.069	1.783	27.243	5.23						1.94	32.3	0.04	0.01					
151	33.911	1.653	27.125	5.69						2.90	29.0	0.28	0.28					
126	33.914	1.876	27.111	5.70						2.95	28.9	0.32	0.24					
91	33.916	1.948	27.107	5.61						2.64	28.4	0.32	0.21					
70	33.898	2.309	27.064	6.28						3.43	26.3	0.29	0.24					
41	33.899	2.627	27.039	6.40						3.96	24.6	0.28	0.05					
10	33.899	2.628	27.038	6.38	3.84	24.5	0.28	0.05										

967

968

Station Name	Lon °E	Lat °S	Seafloor, m	CTD N°	Depth, m	Salinity	Tpot °C	Density, σ_θ	$\delta^{15}\text{N}_{\text{NO}_3}$, ‰	$\delta^{18}\text{O}_{\text{NO}_3}$, ‰	$[\text{NO}_3^-]$, μM	$[\text{NO}_2^-]$, μM	$[\text{NH}_4^+]$, μM					
E4W1	71.43	-48.77	1384	87	1372	34.727	1.922	27.759	4.84	2.26	32.0	0.03	-					
					1204	34.698	2.069	27.724	4.87	1.58	33.1	0.02	-					
					1003	34.638	2.195	27.666	5.07	1.87	34.0	0.02	-					
					903	34.614	2.213	27.645	5.02	2.31	34.4	0.02	-					
					804	34.581	2.226	27.618	4.93	1.61	34.8	0.02	-					
					602	34.516	2.218	27.567	4.92	2.13	35.0	0.02	-					
					449	34.444	2.194	27.510	4.89	1.63	35.1	0.02	-					
					351	34.349	2.102	27.442	5.05	1.60	35.3	0.03	-					
					302	34.262	2.071	27.375	5.10	2.22	34.0	0.03	-					
					160	33.930	1.721	27.135	5.76	2.96	29.6	0.31	-					
					50	33.897	2.561	27.043	6.41	3.93	25.3	0.28	-					
					30	33.897	2.599	27.039	6.47	4.08	24.7	0.28	-					
					E4E	72.56	-48.72	2210	94	903	34.661	2.304	27.676	5.00	1.30	33.9	0.02	-
										702	34.581	2.275	27.614	4.93	1.25	35.1	0.02	-
602	34.526	2.296	27.568	4.92						1.61	35.1	0.03	-					
501	34.459	2.276	27.516	4.95						1.51	36.8	0.03	0.01					
401	34.352	2.236	27.434	5.08						2.15	35.1	0.03	0					
181	33.937	1.808	27.134	5.50						2.71	29.9	0.16	0.11					
150	33.902	1.808	27.107	5.52						-	28.5	0.21	0.31					
126	33.891	1.902	27.091	5.61						3.06	28.6	0.23	0.29					
102	33.874	2.047	27.066	5.74						2.77	27.3	0.26	0.53					
92	33.871	2.096	27.059	5.85						2.77	27.8	0.27	0.50					
51	33.831	3.190	26.935	6.61						3.73	24.5	0.26	0.21					
20	33.831	3.191	26.935	6.66	3.72	24.3	0.26	0.22										

970

971

Station Name	Lon °E	Lat °S	Seafloor, m	CTD N°	Depth, m	Salinity	Tpot °C	Density, σ_θ	$\delta^{15}\text{N}_{\text{NO}_3}$, ‰	$\delta^{18}\text{O}_{\text{NO}_3}$, ‰	[NO ₃], μM	[NO ₂], μM	[NH ₄ ⁺], μM
E4E	72.56	-48.72	2110	97	2194	34.735	1.256	27.815	4.82	2.03	32.6	0.03	-
					2011	34.740	1.403	27.809	5.02	2.56	31.7	0.03	-
					1812	34.744	1.589	27.798	4.93	2.18	31.7	0.03	-
					1506	34.741	1.861	27.775	4.92	2.30	31.2	0.03	-
					1255	34.718	2.066	27.741	5.08	2.22	32.5	0.03	-
					1004	34.675	2.199	27.696	5.00	2.51	34.0	0.03	-
					903	34.654	2.280	27.672	4.98	2.10	34.3	0.03	-
					700	34.576	2.305	27.607	5.07	2.58	35.5	0.03	-
					602	34.516	2.278	27.561	5.05	2.91	35.8	0.03	-
					501	34.442	2.280	27.502	4.93	2.50	36.3	0.03	-
					401	34.360	2.241	27.440	5.05	2.47	-	-	-
					301	34.169	1.863	27.317	5.24	2.59	34.4	0.03	-
					20	33.831	3.222	26.932	6.64	4.68	24.3	0.27	-
A3-2	72.06	-50.62	527	107	509	34.392	2.184	27.470	4.87	2.47	35.4	0.03	0.01
					401	34.288	2.125	27.392	4.87	2.39	35.3	0.03	0.01
					300	34.114	1.906	27.270	5.16	2.54	33.1	0.03	0
					276	34.059	1.804	27.232	5.33	2.98	32.8	0.03	0.02
					201	33.941	1.739	27.143	5.60	4.16	31.1	0.27	0.01
					175	33.918	1.942	27.109	5.76	4.07	28.1	0.36	0.30
					150	33.912	2.153	27.088	6.16	4.07	26.2	0.34	0.26
					126	33.912	2.162	27.087	6.42	4.30	26.2	0.33	0.21
					81	33.912	2.162	27.087	6.40	4.66	26.0	0.33	0.21
					39	33.911	2.242	27.080	6.41	4.62	25.7	0.33	0.17
11	33.911	2.252	27.079	6.46	4.25	25.2	0.33	0.19					

973

974

975 Table A1: Continued

Station Name	Lon °E	Lat °S	Seafloor, m	CTD N°	Depth, m	Salinity	Tpot °C	Density, σ_θ	$\delta^{15}\text{N}_{\text{NO}_3}$, ‰	$\delta^{18}\text{O}_{\text{NO}_3}$, ‰	[NO ₃], μM	[NO ₂], μM	[NH ₄ ⁺], μM
E4W2	71.43	-48.77	1390	111	802	34.568	2.225	27.608	4.64	2.44	34.4	0.02	-
					601	34.502	2.227	27.554	5.45	3.39	34.9	0.03	-
					501	34.440	2.196	27.508	4.75	2.64	34.9	0.03	-
					401	34.378	2.166	27.460	5.09	3.41	34.3	0.03	0
					300	34.261	2.020	27.378	5.40	3.24	33.8	0.03	0
					251	34.173	1.897	27.317	5.07	2.45	33.1	0.04	0
					201	34.087	1.792	27.256	5.01	3.46	33.4	0.04	0.01
					126	33.902	1.829	27.105	5.54	3.84	-	-	-
					126	33.899	1.893	27.098	5.39	3.85	28.0	0.25	0.60
					100	33.884	2.245	27.058	6.41	4.79	26.4	0.27	0.77
					75	33.880	2.551	27.030	6.91	5.14	24.4	0.28	0.56
					50	33.872	2.815	27.001	7.40	-	23.1	0.28	0.18
					11	33.837	3.076	26.950	7.02	5.16	23.3	0.26	0.06
E5	71.90	-48.41	1920	113	1906	34.743	1.554	27.800	4.90	2.31	32.0	0.03	-
					1204	34.716	2.107	27.736	5.06	2.05	32.5	0.03	-
					1003	34.672	2.210	27.692	5.00	1.39	33.5	0.03	-
					904	34.642	2.241	27.665	4.98	1.73	34.1	0.03	-
					803	34.611	2.252	27.640	5.05	2.12	34.9	0.03	-
					602	34.504	2.249	27.554	5.12	1.82	35.7	0.03	-
					501	34.450	2.208	27.514	5.11	1.47	35.4	0.03	-
					452	34.410	2.203	27.483	5.07	1.90	35.3	0.03	-
					401	34.365	2.153	27.451	5.09	1.92	34.4	0.03	-
					220	34.001	1.764	27.189	5.42	2.99	30.9	0.11	-
					101	33.854	2.736	26.994	6.32	3.87	26.2	0.27	-
					51	33.847	3.087	26.957	6.70	4.80	25.7	0.26	-

976

977

978 Table A1: Continued

Station Name	Lon °E	Lat °S	Seafloor, m	CTD N°	Depth, m	Salinity	Tpot °C	Density, σ_θ	$\delta^{15}\text{N}_{\text{NO}_3}$, ‰	$\delta^{18}\text{O}_{\text{NO}_3}$, ‰	$[\text{NO}_3^-]$, μM	$[\text{NO}_2^-]$, μM	$[\text{NH}_4^+]$, μM
E5	71.90	-48.41	1920	114	903	34.640	2.245	27.663	5.07	1.97	34.0	0.03	-
					702	34.559	2.245	27.599	5.12	2.00	35.0	0.03	-
					601	34.504	2.250	27.554	5.09	2.29	35.4	0.03	-
					503	34.454	2.216	27.517	5.17	2.04	36.3	0.03	-
					402	34.365	2.153	27.451	5.10	1.97	35.6	0.03	0
					300	34.211	1.940	27.344	5.16	1.95	34.0	0.03	0
					250	34.099	1.818	27.264	5.29	2.43	32.9	0.04	0
					202	33.911	1.822	27.113	5.71	3.59	29.4	0.3	0.32
					150	33.892	1.954	27.088	6.04	3.52	28.1	0.31	0.57
					125	33.889	2.082	27.075	6.07	4.07	28.0	0.3	0.63
					101	33.875	2.128	27.060	5.76	3.60	27.9	0.31	0.53
					82	33.849	2.989	26.967	6.46	4.71	25.8	0.26	0.54
					41	33.846	3.092	26.956	6.57	3.95	25.3	0.25	0.45
					11	33.836	3.257	26.932	6.56	3.94	25.0	0.25	0.28

979

980

981

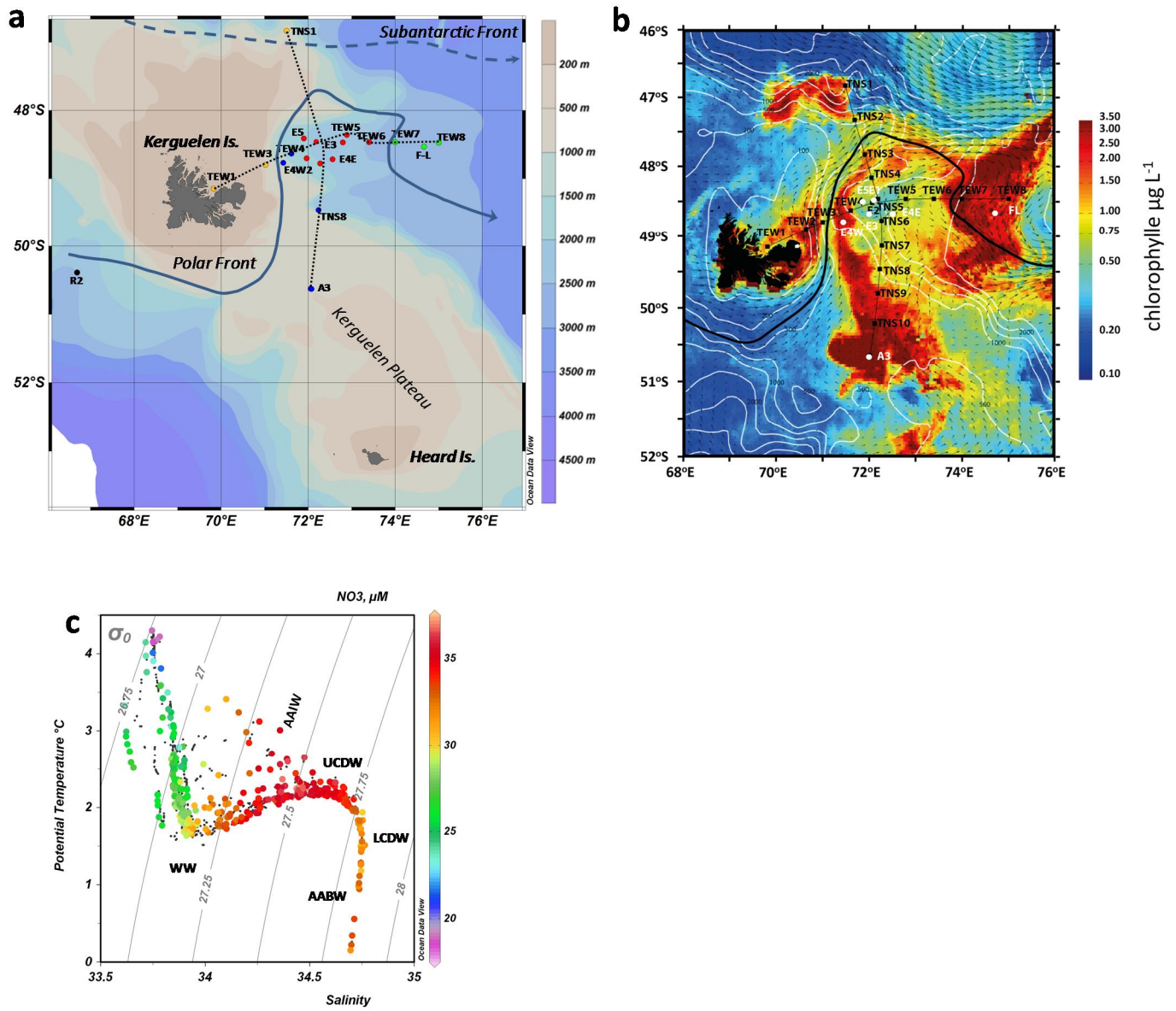
982 Table A1: Continued

Station Name	Lon °E	Lat °S	Seafloor, m	CTD N°	Depth, m	Salinity	Tpot °C	Density, σ_θ	$\delta^{15}\text{N}_{\text{NO}_3}$, ‰	$\delta^{18}\text{O}_{\text{NO}_3}$, ‰	$[\text{NO}_3^-]$, μM	$[\text{NO}_2^-]$, μM	$[\text{NH}_4^+]$, μM
IODA	72.89	-48.36	2300	120	2278	34.732	1.171	27.818	5.03	2.63	32.7	0.03	-
RECOVERY					2011	34.742	1.418	27.809	5.00	2.25	31.7	0.02	-
					1809	34.746	1.615	27.798	5.02	1.72	31.7	0.02	-
					1606	34.744	1.797	27.783	4.92	2.42	31.8	0.02	-
					1205	34.714	2.098	27.735	5.08	1.86	33.0	0.02	-
					1003	34.672	2.188	27.694	5.03	1.97	33.7	0.02	-
					702	34.582	2.315	27.611	5.04	1.61	34.8	0.03	-
					602	34.529	2.324	27.568	5.16	2.44	35.1	0.03	-
					501	34.464	2.339	27.515	5.25	2.13	36.6	0.02	-
					399	34.347	2.199	27.432	4.99	2.16	35.1	0.02	-
					350	34.300	2.166	27.398	5.16	3.32	36.1	0.03	-
					300	34.239	2.114	27.352	5.21	2.29	34.2	0.03	0.01
					251	34.150	2.037	27.288	5.22	2.34	32.6	0.03	0.01
					201	34.060	1.980	27.220	5.38	2.68	31.5	0.05	0.00
					148	33.921	1.882	27.116	5.54	3.27	29.7	0.12	0.03
					79	33.839	2.752	26.980	6.12	5.15	26.7	0.28	0.66
					50	33.822	3.329	26.915	6.77	4.88	24.4	0.26	0.62
					12	33.819	3.543	26.892	6.99	5.43	23.5	0.26	0.24

983

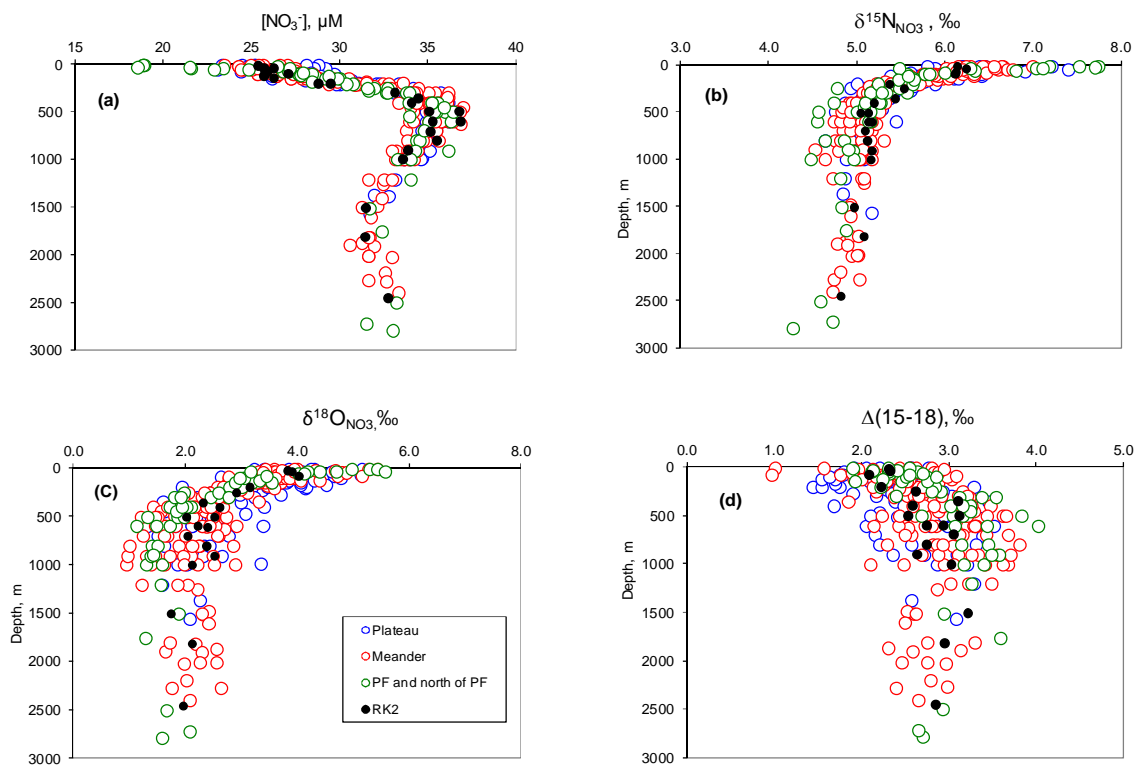
984

985



986
 987
 988 Figure 1

989
 990

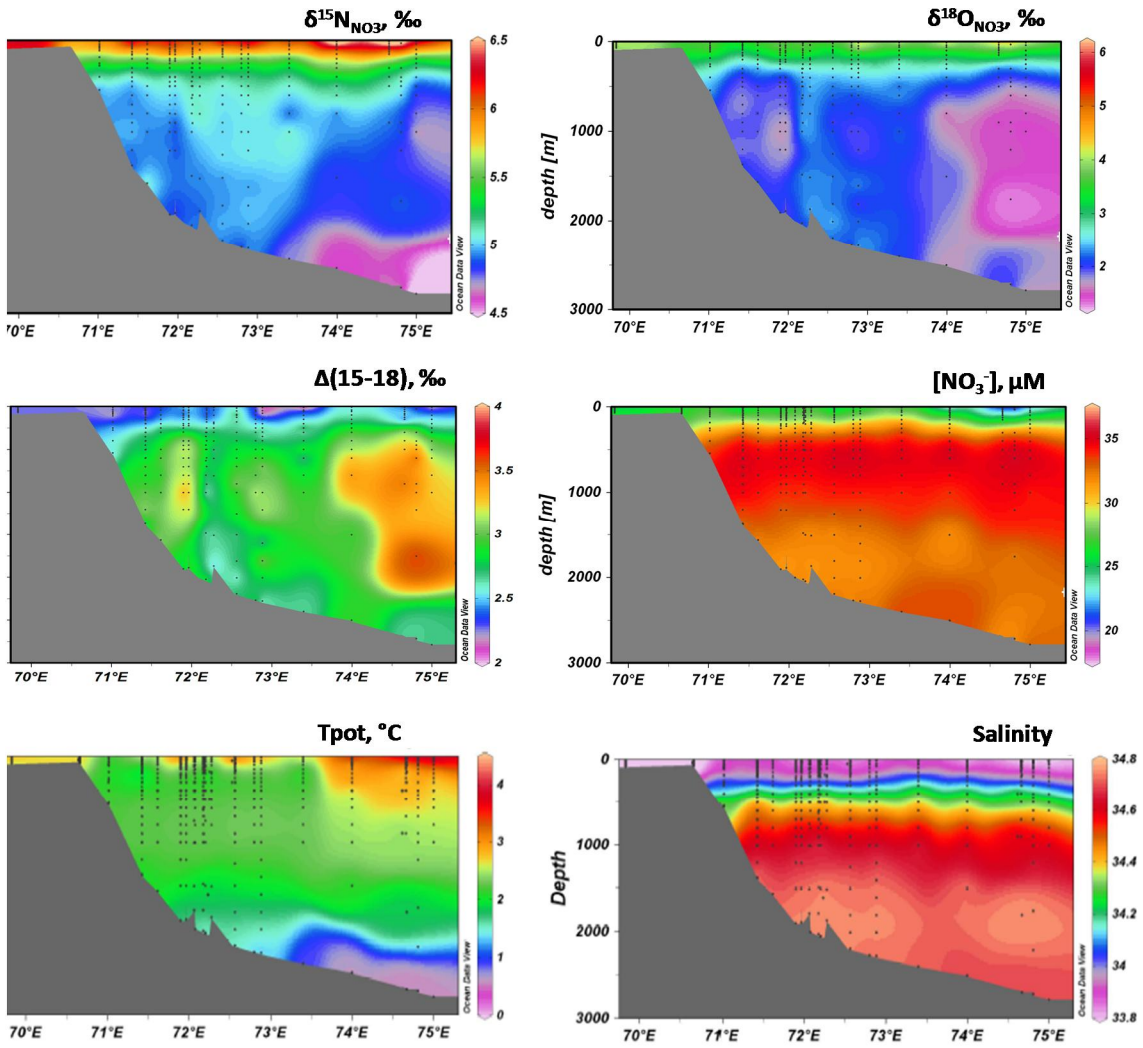


991

992

993 Figure 2

994

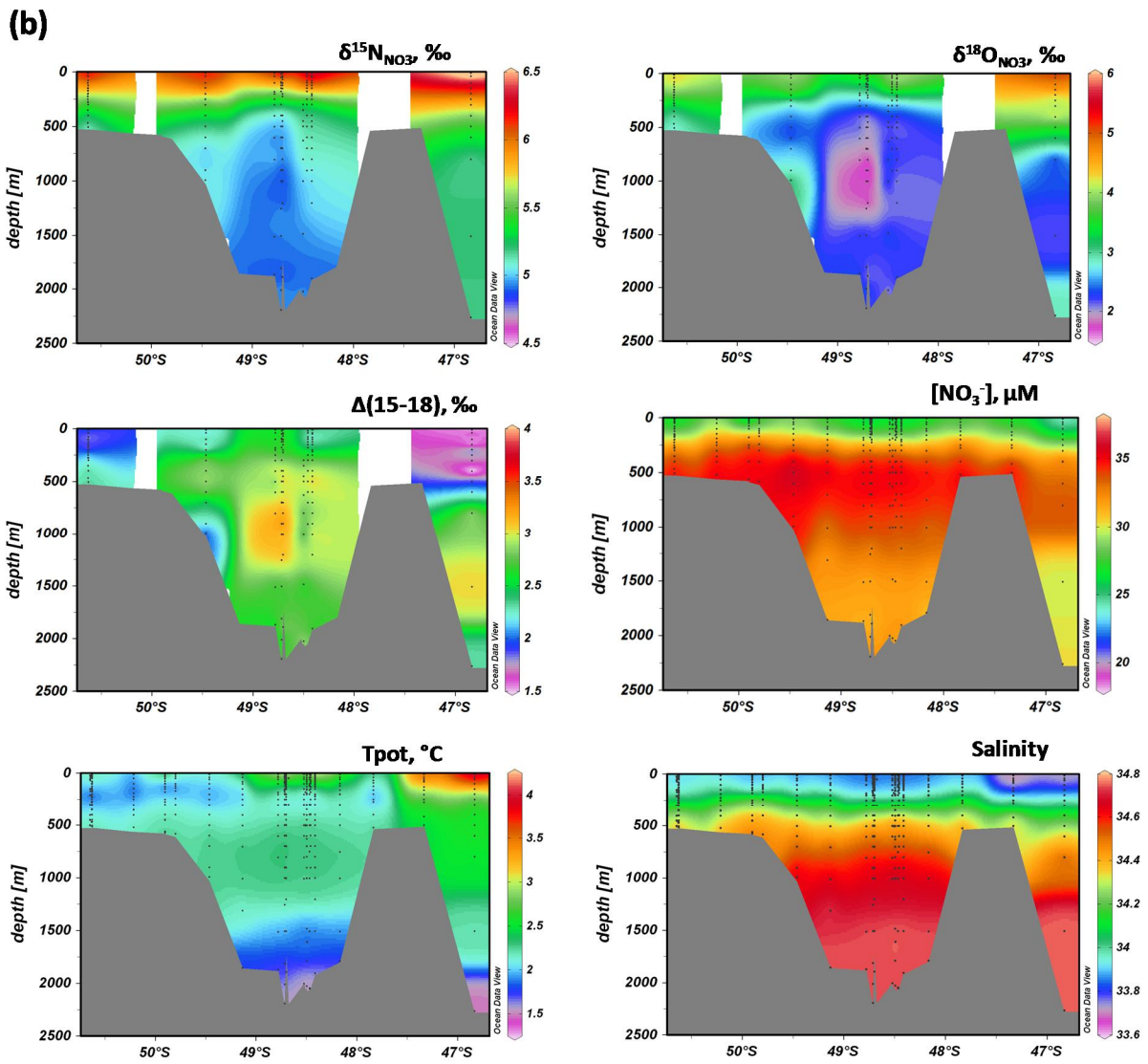


995

996

997 Figure 3a

998

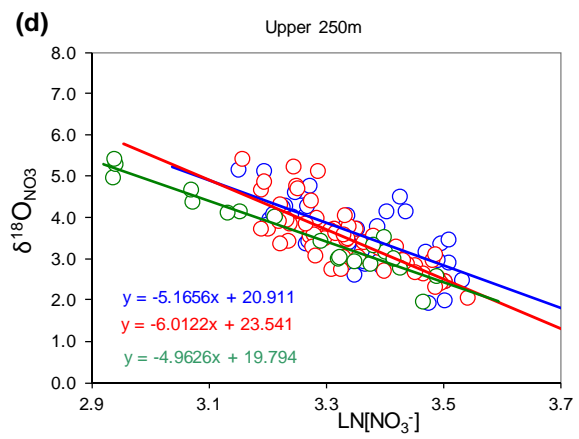
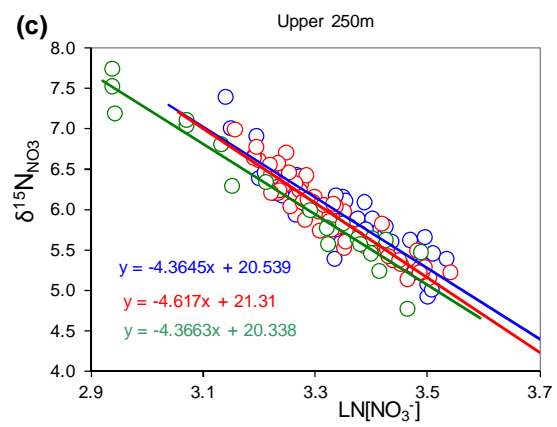
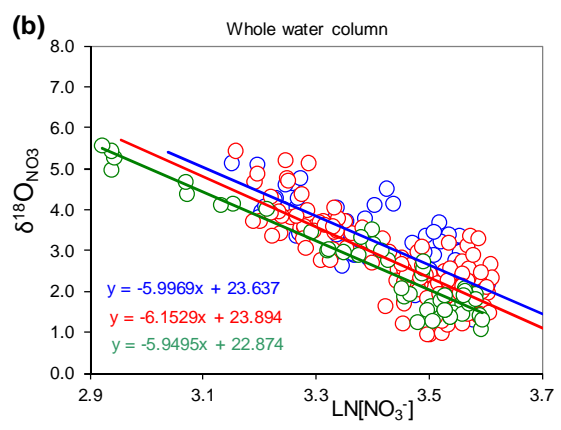
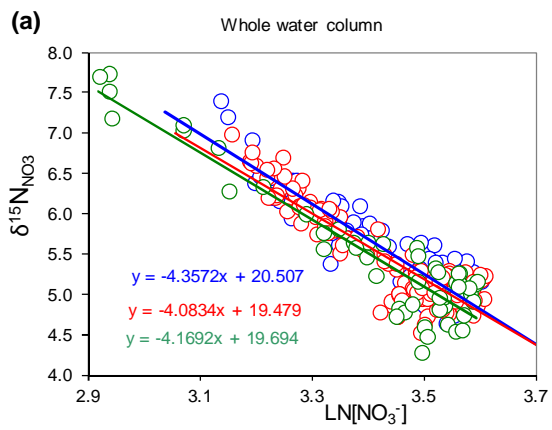


999

1000

1001 Figure 3b

1002

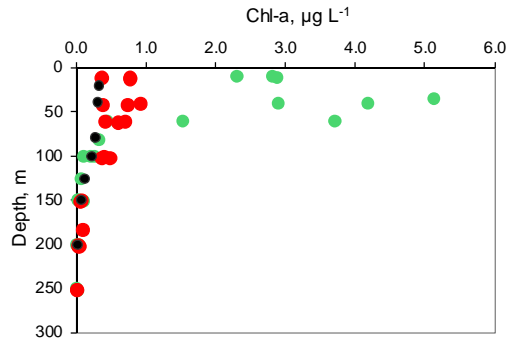
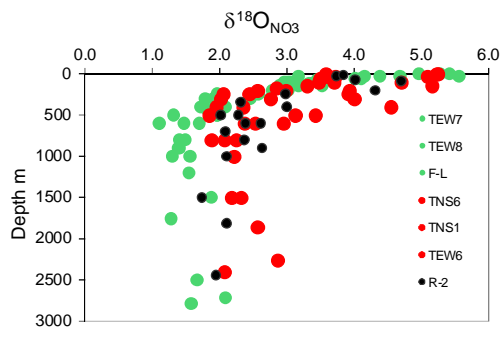


1003

1004

1005 Figure 4

1006

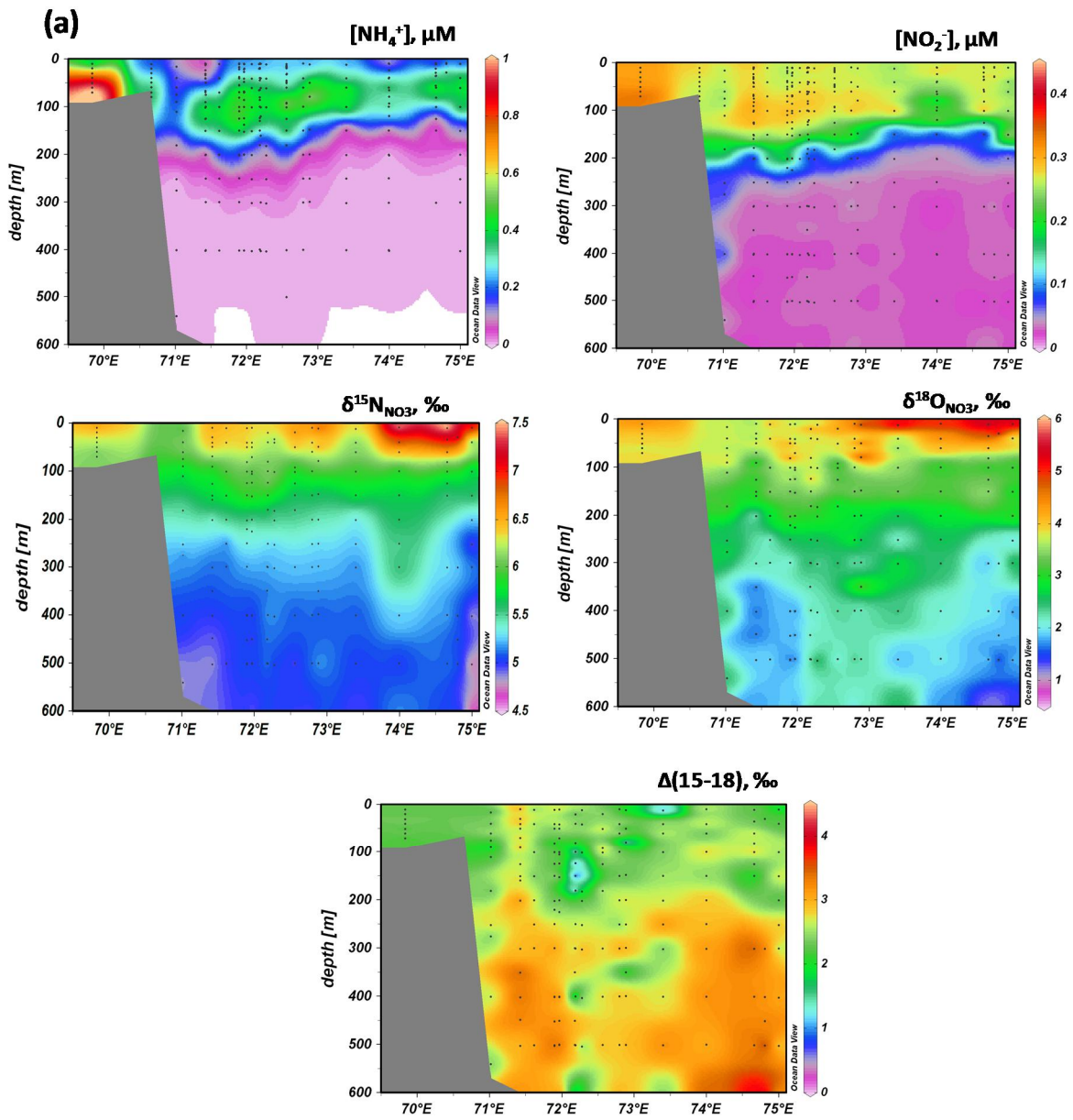


1007

1008

1009 Figure 5

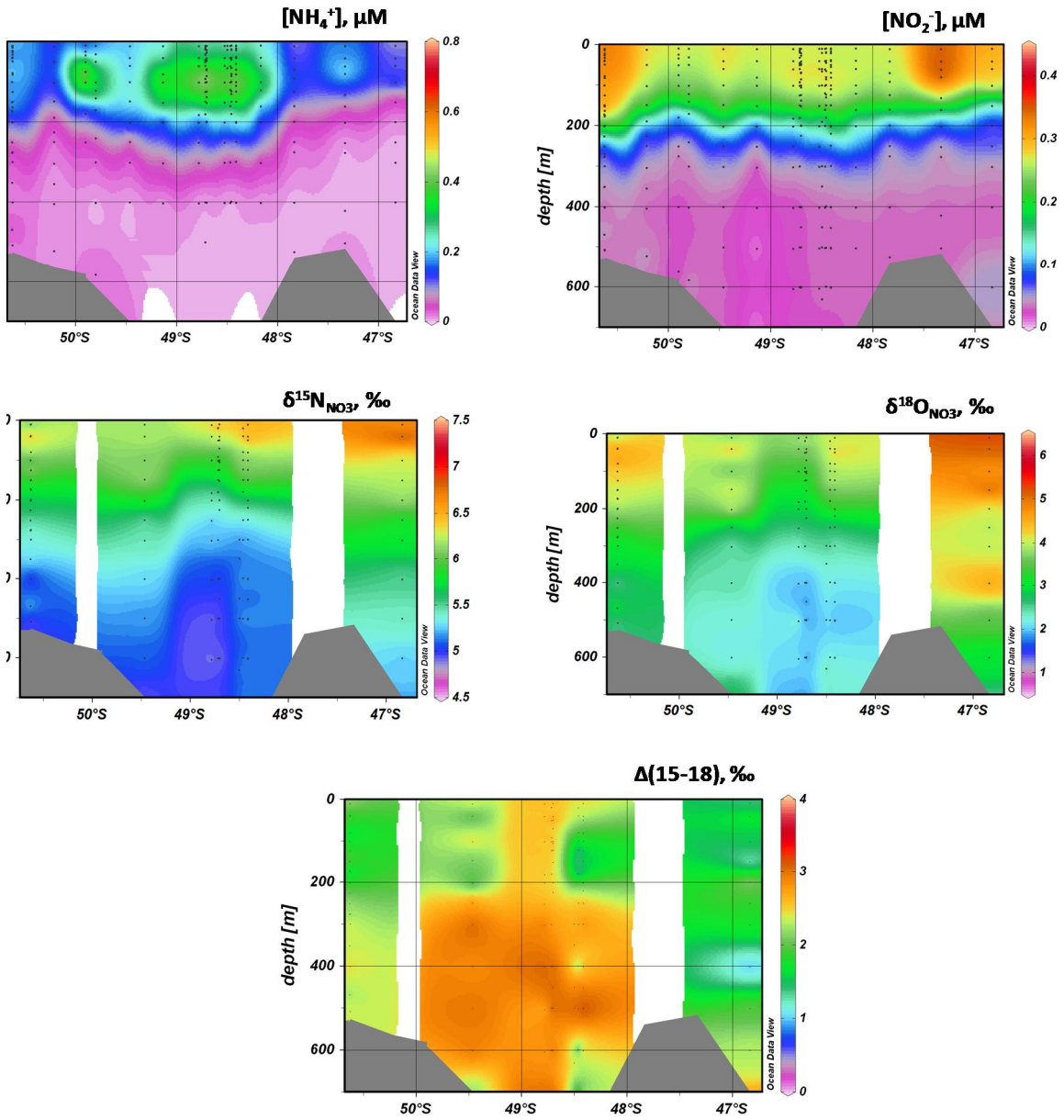
1010



1011

1012 Figure 6a

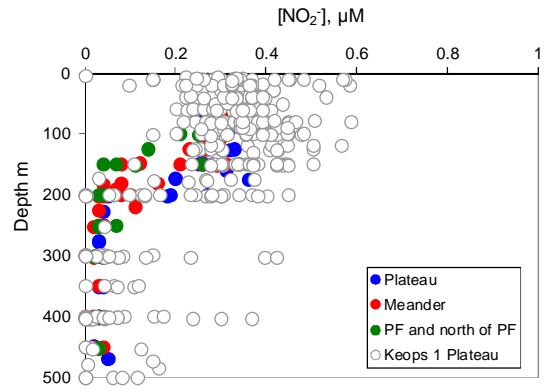
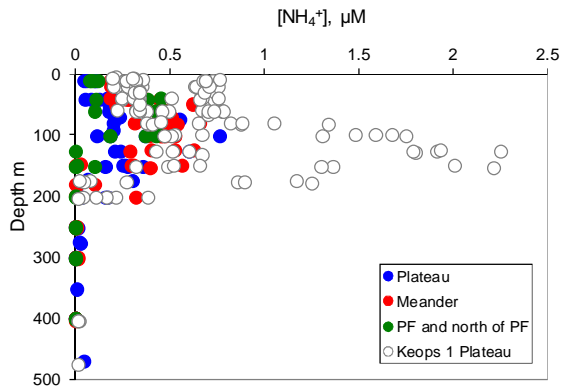
1013



1014

1015 Figure 6b

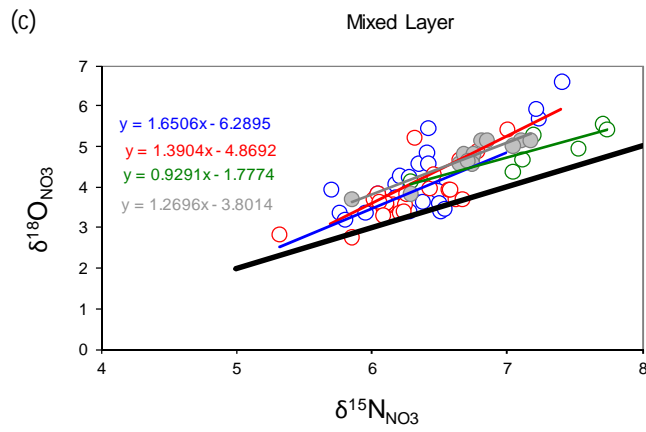
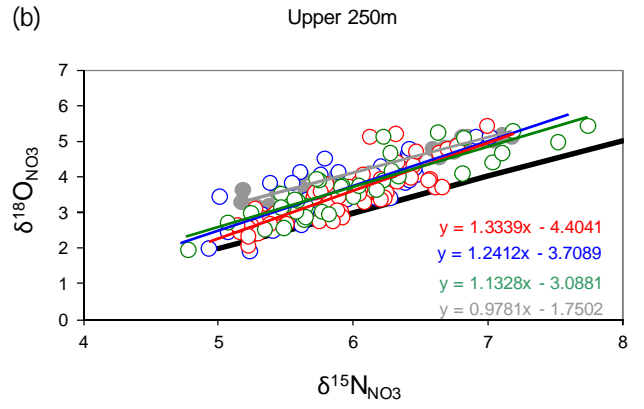
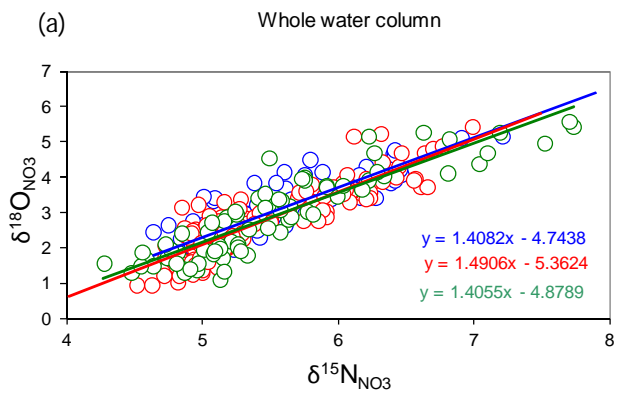
1016



1017

1018 Figure 7

1019



1020

1021

1022 Figure 8

1023

1024